Review article

Institution of MECHANICAL ENGINEERS
Journal of MATERIALS: DESIGN AND APPLICATIONS

Proc IMechE Part L:
J Materials: Design and Applications
0(0) 1–43

DOI: 10.1177/14644207211010839
journals.sagepub.com/home/pil
SAGE

Solid-state joining of aluminum to titanium: A review

Vijay S Gadakh[1], Vishvesh J Badheka[2] and Amrut S Mulay[3]

Abstract

The dissimilar material joining of aluminum and titanium alloys is recognized as a challenge due to the significant differences in the physical, chemical, and metallurgical properties of these alloys, where the increasing demands for high strength and lightweight alloys in aerospace, defense, and automotive industries. Joining these two alloys using the conventional fusion techniques produces commercially unacceptable sound joints due to irregular, complex weld pool shapes, cracking and low strength, high residual stresses, cracks, and microporosity, and the brittle intermetallic compounds formation leads to poor formability or inferior mechanical properties. The formation of intermetallic compounds is inevitable but it is less severe in solid-state than in the fusion welding process. Hence, this article reviews on aluminum–titanium joining using different solid-state and hybrid joining processes with emphasis on the effect of process parameters of the different processes on the weld microstructure, mechanical properties along with the type of intermetallic compounds and defects formed at the weld interface. Among the various solid-state welding processes for aluminum–titanium joining, the following grades of aluminum and titanium alloys were employed such as cp Ti, Ti6Al4V, cp Al, AA1xxx, AA 2xxx, AA5xxx, AA6xxx, AA7xxx, out of which Ti6Al4V and AA6xxx alloys are the most common combination.

Keywords

Aluminum, titanium, solid-state, hybrid, dissimilar welding, intermetallics, microstructure, weldability

Date received: 6 December 2020; accepted: 30 March 2021

Introduction

Aluminum (Al) and titanium (Ti) alloys are lightweight workhorse materials among other aerospace and automobile industries. Ti and its alloys find several applications because of their better mechanical properties in aircraft and biomedical applications. Owing to these attractive properties for Al is popular in several practical applications. With this, Al to Ti alloy joining is employed in aerospace, automobile,[1–23] marine,[7,8,16] and defense industries[18,24] where current efforts are being made to ensure more values of strength-to-weight ratio and are attained at an affordable price. For instance, in aircraft manufacturing, the welding of riveted fuselage structures are replaced by skin stringer joints,[23,25] seat track,[22,25–28] heat exchangers[7,8] or electric conductors in corrosive media,[29] tubing and pipework of propellant tanks,[30] medical industry,[2] architecture,[1] joining the Al skins to Ti ribs for aircraft,[31] aircraft structural parts,[32] joining of Ti alloy crust and Al alloy honeycomb (wing of airplanes),[27,33] cooling fin employed in aeroplane cabins are made from welding of Al and Ti,[27] experimental NASA YF-12 fighter wings,[27] transportation industries,[34–38] chemical industries,[39] cryogenics, nuclear, and thermal power station.[40] Further, there is another possibility of implementation of hybrid structures[41–43] i.e. tailored welded blanks.

Ti is well known for a structural material application having high specific and high-temperature strength within a broad temperature range from deep-freeze temperatures (cryogenic alloys) up to 500–600°C (high-temperature alloys); high corrosion resistance. Thermal management issues become more important while welding Ti with Al alloys. The two

[1]Department of Mechanical Engineering, Amrutvahini College of Engineering, Sangamner, Ahmednagar, India
[2]Department of Mechanical Engineering, School of Technology, Pandit Deendayal Energy University, Raisan, Gandhinagar, India
[3]Department of Mechanical Engineering, Sardar Vallabhbhai National Institute of Technology, Ichchanath, Surat, India

Corresponding author:
Vijay S Gadakh, Department of Mechanical Engineering, Amrutvahini College of Engineering, Sangamner, Ahmednagar 422 608, Maharashtra, India.
Email: vijay.gadakh@avcoe.org

materials not only differ considerably in their melting point (above 1600°C for Ti alloys and below 660°C for Al alloys) but their thermal conductivities also differ considerably (0.041 for Ti and 0.49 cal/cm-s-°C for Al), though the joining of dissimilar Al to Ti alloys is considered an important issue, because of considerable variation in diverse properties of the Al and Ti alloys involved.[44] A few of the general problems related with the Al to Ti welds via traditional fusion processes are inferior metallurgical properties owing to uneven, intricate weld pool profiles, cracking and low strength, particularly for alloys, high residual stresses, cracks, and microporosity[26] and brittle intermetallic compounds (IMC) formation with its shape, size, and distribution. The IMC formation reduces the joint performance depending on its thickness. Hence, solid-state joining performs a vital part over conventional fusion welding. The formation of IMC is inevitable but its percentage is less in the case of solid-state joining than fusion joining.[45] For any of the joining processes, the optimal window of process parameter is the primary requirement.[46]

Many IMCs are formed in the binary Ti–Al system namely, Ti_3Al, TiAl, Al_3Ti, $TiAl_2$, Ti_5Al_{11}, and Ti_9Al_{23}. It has been studied that only Al_3Ti having higher free energy formed as the diffusion product due to exothermic chemical reaction at Al–Ti interface[47] during the Al–Ti reaction at high temperatures (700–1000°C).[48]

To date, Al and Ti welds are not found acceptable joints with desired strength using fusion welding as a commercially acceptable joint due to the above-mentioned issues. To avoid the issues of fusion welding of the Al–Ti system solid-state welding has been employed and is discussed in this paper. Solid-state and hybrid welding process classification based on published literature for joining Al–Ti alloys is depicted in Figure 1 and Figure 2 shows the number of referred papers of different solid-state and hybrid welding processes adopted for joining Al–Ti alloys. From Figure 2 it is seen that maximum researchers have used friction or deformation-based welding process.

Literature review

This section is divided based on the various processes like friction welding (FW), friction stir lap welding (FSLW), friction stir butt welding (FSbW), friction stir spot welding (FSSW), diffusion bonding, and other related processes employed for joining Al and Ti alloys along with their process parameters, tool design, materials, their effect on microstructure–mechanical properties.

Friction welding

It is a variant of a solid-state welding process where the joint is produced through heating the faying surfaces with mechanical friction between a rotating and stationary component with applied lateral upset force against the parts depicted in Figure 3. The process is also known as inertia, rotational, inertial FW as no melting occurs. It is widely used for metals, thermoplastics in aviation, automotive, and other similar applications.[49] The process parameters which affect the weld quality are explained in Table 1. These process parameters are explained in detail for the Al–Ti welds using FW.

Friction pressure. Fuji et al.[51] studied the influence of FW and after-weld heat treatment on the mechanical and metallurgical properties of cp Ti and AA5083 alloy and it is claimed that the highest strength joint achieved with friction pressure (FP) 230 MPa and friction time (FT) of 0.5 s without intermetallic formation at the bond line.

Friction time. Fuji et al.[51] argued that the decrease in joint tensile strength observed when FT increased from 0·5 to 3 s at FP 230 MPa. The growth of the intermediate growth layer for cp Ti–cp Al was studied by changing FT at 2 s and 7 s.[53] It is observed that the growth rate of the layer does not show a parabolic or linear time dependence. Only a small variation in layer growth rate was found between the central and circumferential joint region with FT 2 and 7 s.

Rotational speed. Hynes and Velu[2] studied the effect of rotational speed (RS) on the joint properties at the FW interface of Ti6Al4V and AA6061 alloys. It is claimed that RS is a crucial process parameter that influences the metallurgical properties of the joint. The intermixed zone and its thickness formation are based on the choice of RS. It is argued that an increase in RS increased the brittle interlayer thickness (probably Al_3Ti). Further, the interface of weld shows high hardness than Ti parent metal as can be seen in Figure 4, due to the effect of RS and the formation of the inter-mixed zone at the joint interface. Regarding Al, the average hardness is increased by ~5% in contrast to the heat-affected zone (HAZ) because of the eutectic formation with fine recrystallized grains, which are formed due to the influence of heat input (HI) and RS. Kimura et al.[1] evaluated the tensile properties of the FWed joint of Ti6Al4V–AA5052–H112 alloy and Ti6Al4V–AA5052–H34 alloy. It is claimed that 100% joint efficiency for Ti6Al4V–AA5052–H112 joints at RS: 1650 r/min, FP: 30 MPa, FT: 3.0 s, and upset pressure (UP): 60 MPa, whereas for Ti6Al4V–AA5052–H34 joints 100% joint efficiency at RS: 1650 r/min, FP: 150 MPa, FT: 0.5 s, and UP: 275 MPa was attained.

Metallurgical properties. Fuji et al.[51] do not observe the intermetallic formation at the bond line in as-welded Ti-5083 joints using FT: 0.5 s and FP: 230 MPa. However, at FT: 3 s and FP: 160 MPa, a 200 nm the intermetallic layer thickness (only τ-Al, i.e.

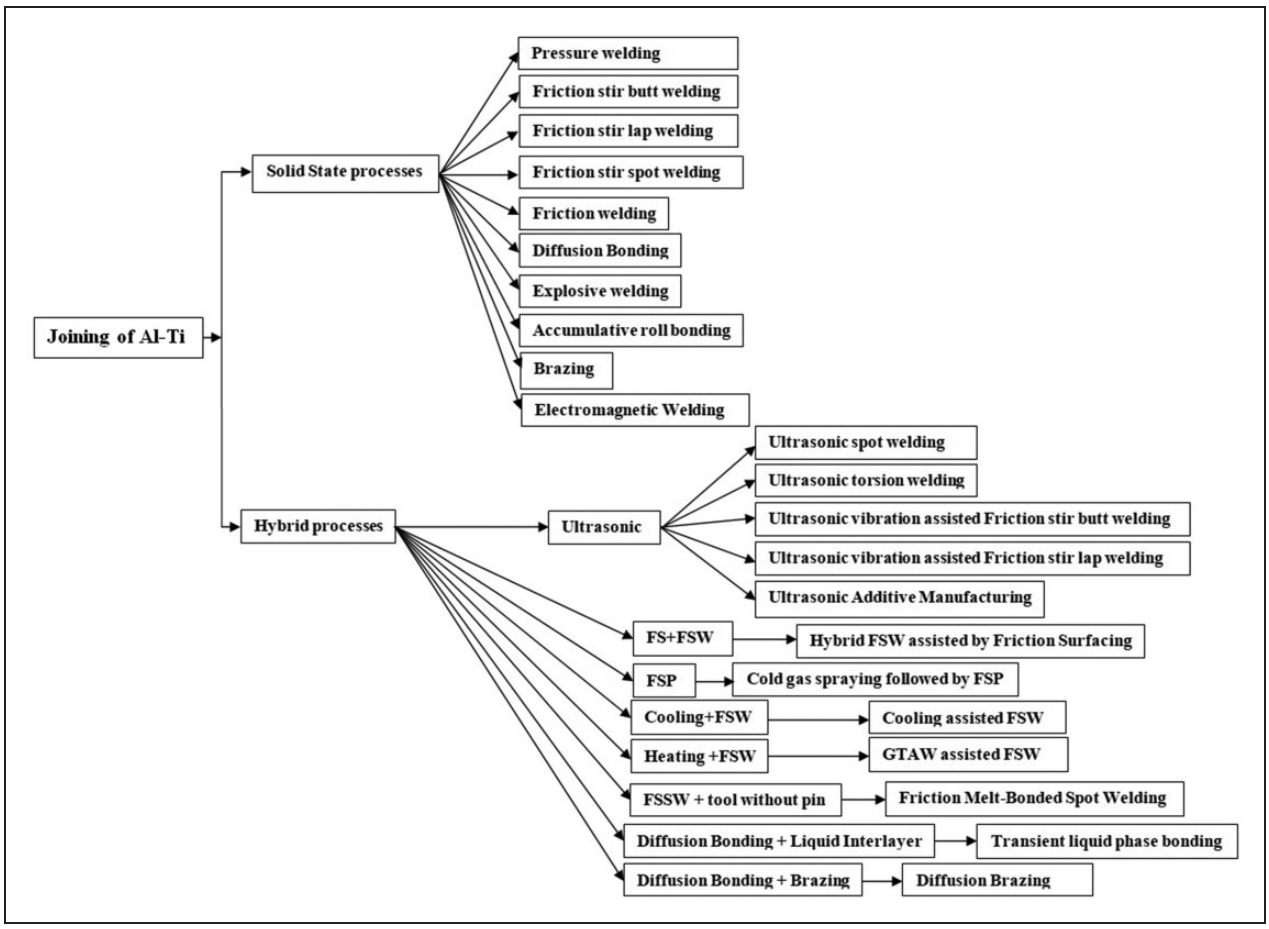

Figure 1. Different solid-state and hybrid welding processes reported for joining Al–Ti alloys.
FS: friction surfacing; FSW: friction stir welding; FSP: friction stir processing; FSSW: friction stir spot welding.

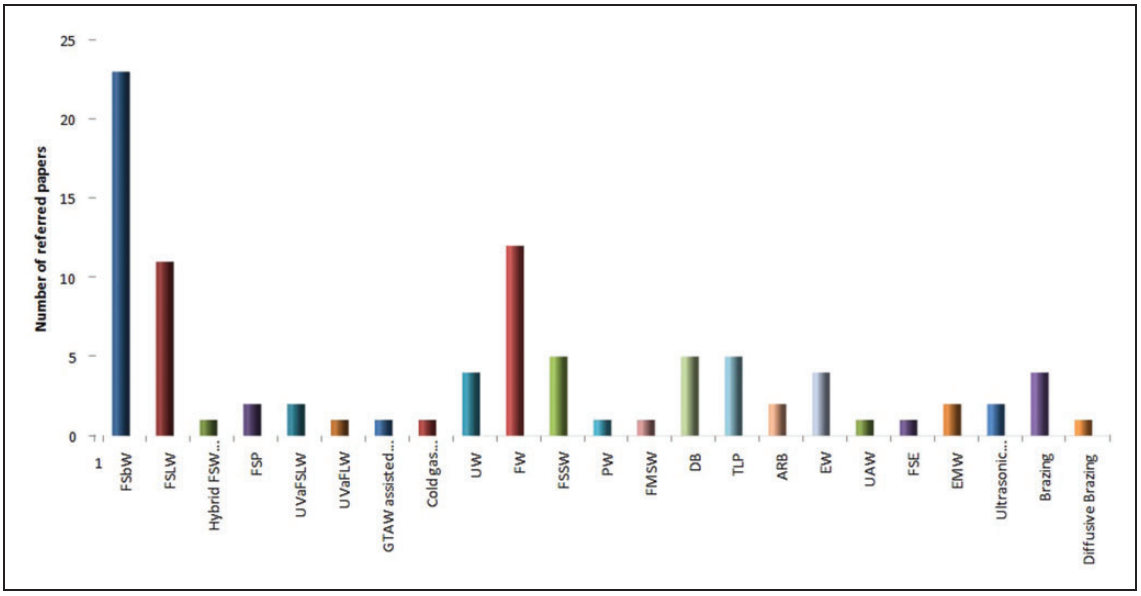

Figure 2. The number of referred papers of different solid-state and hybrid welding processes adopted for joining Al–Ti alloys.
FSbW: friction stir butt welding; FSLW: friction stir lap welding; FSW: friction stir welding; FSP: friction stir processing; UVaFSLW: ultrasonic vibration-assisted friction stir lap welding; UVaFLW: ultrasonic vibration-assisted friction stir butt welding; GTAW: gas tungsten arc welding; UW: ultrasonic welding; FW: friction welding; FSSW: friction stir spot welding; PW: pressure welding; FMSW: friction melt-bonded spot welding; DB: diffusion bonding; TLP: transient liquid phase bonding; ARB: accumulative roll bonding; EW: explosive welding; UAW: ultrasonic-assisted welding; FSE: friction stir extrusion; EMW: electromagnetic or magnetic pulse welding.

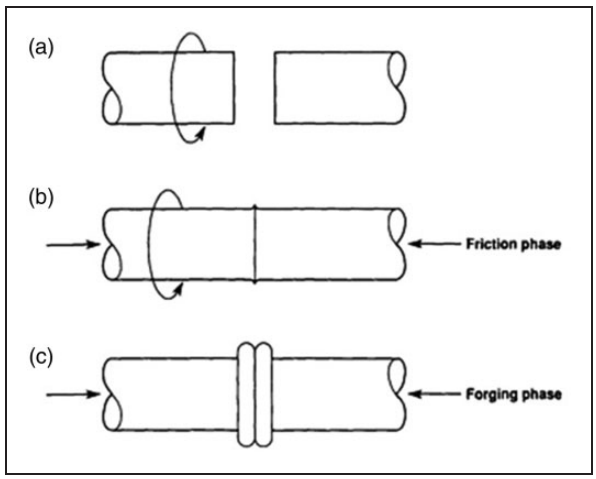

Figure 3. A schematic diagram of the friction welding process.

$Ti_2Mg_3Al_{18}$) formed at the bond line and post-weld heat-treated joints at 450°C for 3·6 ks. Related work is reported by Kimura et al.[1] when FT was longer and joints were fractured at the welded interface. Further, they claimed that defect-free joints with better metallurgical properties were achieved for the joints made with high FP, short FT, and high UP. It has also been observed that at FP: 230 MPa with an increase in FT from 0.5 s to 3.0 s with a decrease in tensile strength and growth creation of a brittle interfacial layer ($Ti_2Mg_3Al_{18}$) at the joint interface. According to Kim and Fuji,[55] the major factor deciding the joint characteristics is the Al_3Ti IMC layer thickness mainly produced at the Al substrate interface, not the mechanical factors. For the post-weld heat-treated joints with longer working times, the joint performance is greatly reduced as the IMC layer thickness increases. The critical IMC thickness was found about 5 μm, which decides the tensile strength and the bending ductility. Recently, Velu et al.[55] joined AA6061/Ti6Al4V with Zn interlayer and found that at 1000 r/min and 0.5 mm interlayer thickness, defect-free and sound joints with improved joint strength and minimum IMC layer thickness were achieved. Hynes and Velu[57] have done numerical studies and the influence of variables on thermal evolution and axial shortening of the joints. It is claimed that the Al–Ti joint interface temperature is 475°C, which gradually increased and was nonuniformly distributed across the interface. Kim et al.[56] claimed that the dominant factors for joining Al–Ti are not the mechanical factors rather these are metallurgical (i.e. the thickness of IMC layer) one as the residual stresses and plastic strains produced during welding are small. It is also suggested that the IMC layer thickness gets increased if the joint is utilized in an elevated thermal atmosphere.

To conclude, for maximum tensile strength of dissimilar FWed joints of Al-Ti alloys, it is recommended that a minimum of ~5 μm the IMC thickness is suitable. This is achieved through control of the process parameters like FP, FT, and RS. It is suggested that the joints with high FP, short FT, and high UP gives good mechanical and metallurgical properties. The use of an interlayer is also suggested for the improvement in joint strength. However, tensile strength is nearly the same either with or without the use of an interlayer.

Friction stir butt welding

FSW is a modified form of the traditional FW process wherein a joint is produced by deformation and frictional heat using a tool having specialized shoulder design and pin features as shown in Figure 5. It is observed demonstrably superior compared to conventional welding techniques due to its solid-state nature as well as its energy efficiency, environment friendliness, and versatility and hence, find a range of applications in areas like automobile, marine, railway, aerospace, etc.

According to the joint configuration in the current context, it is classified as FSbW, FSLW, and FSSW. There is a slight difference in FSLW and FSSW; i.e. in the former case, joint produced is by a continuous weld in lap configuration using combinations of vertical force (VF), tool rotational speed (TRS), and weld speed (WS), whereas in the latter case the joint is obtained by a series of spot weld in lap configuration using VF and TRS with dwell time (DT). Depending upon the application and need, these processes are used. Each process has a diverse range of applications in different areas. FSW process is widely employed in welding-related and different alloys and materials. The FSbW process variables which affect the weld quality and joint strength are shown in Table 2. These parameters are explained in detail concerning the Al–Ti welds using FSbW.

Tool material. The tool material selection is a crucial criterion for obtaining sound quality of joint with no or less tool wear and minimum cost.[68] It depends mainly on workpiece material and thickness to be weld, ease of machinability with the least cost. Following tool materials are reported for FSbW of Al–Ti welds as WC-based alloy tool,[13] WC-12 Co,[41,60] WC-8% Co,[17–20,24,25,61] SKD61 850,[3] SKD61,[4] WC-Co,[21,22,34] WC-13 wt% Co for "L"-shaped modified joint,[23] HSS for intercalated butt joint,[65] standard tool steel with coated shoulder and pin,[42] and WC.[63] Most of the referred literature suggested WC-based alloy materials but other W-based tools like W-Re and polycrystalline cubic boron nitride (PCBN) were not reported so far where these are best tool materials for deeper penetration welds of high-temperature materials with high-temperature stability. However, it has been suggested that the performance of W-Re and PCBN tools are promising but the manufacturing cost is very high.[69] Also, to avoid

Table 1. Summary of suggested parameters and findings of Al–Ti friction welding.

WP materials	Parameters	Interlayer	Findings	Ref.
AA5052–H112–Ti6Al4V AA5052–H34–Ti6Al4V	D: 12 mm, FP: 30 MPa, FT: 3 s, RS: 342, 678, 1050, 1650, 3000 r/min, UP: 60 MPa, UT: 6 s	–	JE: 100% for Ti6Al4V–AA5052–H112 joint at 678, 1050, 1650 r/min. JE: 100% for Ti6Al4V–AA5052–H34 joint at 1650 r/min, FP: 150 MPa, FT: 0.5 s, UP: 275 MPa. Joints with high FP, short FT, and high UP shows good mechanical and metallurgical properties.	1
AA 6061 T6–Ti6Al4V	D: 25 mm (Al) and 16 mm (Ti), RS: 800, 1000, 1200 r/min	–	Highest TS: 186.59 MPa and impact strength: 8J, micro hardness: 413.8HV0.5 at RS: 1000 r/min.	2
AA6082–T651–Ti6Al4V	D: 12 (Al), 8 (Ti) mm, Friction force: 9–18 kN, FT: 3000 ms (max.), RS: 6000–14,000 r/min, UP: 13–30 kN, UT: 250–2500 ms, Contact force: 500 N.	–	No direct evidence for the $TiAl_3$ IMCs formation.	30
Al (6×10^{-4} wt% Si and 0.12 wt% Si)–Ti	FP: 50 MPa; FT: 2 s; UP: 100 MPa and UT: 6 s., D: 12 mm	–	TS and bend test properties of Ti/0.12 wt% Si A1 joints markedly decreased by heat treatments with shorter holding times at lower temp. Joint failure in both joints occurred when the width of the intermediate layer formed exceeds $\sim$10 μm. Si segregation acts as a barrier that retards $A1_3Ti$ formation.	50
cp-Ti–Al 5083	FP: 160–230 MPa, FT: 0·5, 1, 2, 3 s, RS: 1500 r/min, UP: 330 MPa, UT: 6 s	–	Highest TS at FT: 0.5 s, FP: 230 MPa with no Intermetallic phase formation, TS markedly decreased when a 200 nm intermetallic layer thickness formed at the bond line at FT: 3 s, FP: 160 MPa.	51
cp-Ti–Al-1.03 mass–%Mn and Al–4.63 mass–%Mg	D: 17 mm, FP: 50 MPa, FT: 2s, RS: 1500 r/min, UP: 50 MPa, UT: 6 s	–	For the Ti/Al–Mg joint the growth rate of the interlayer is much faster rapid more than the Ti/Al–Mn joint. The growth nature of interlayer for Ti/Al–Mn alloy joint from Al to Ti side whereas for Ti/Al–Mn joint it is from the Ti-Al side. For both joints, no exact relations fitted for the growth rate of the interlayer.	52
Al (0.01 wt% Si and 0.12 wt% Si)–cp Ti	D: 30 mm, FP: 50 MPa, FT: 2 and 7s, RS: 1500 r/min, UP: 50 MPa, UT: 6 s	–	For both joints, no exact relations fitted for the growth rate of the interlayer, The layer growth rate of the cp Ti – 0.01 wt % Si Al joints higher than cp Ti – 0.12 wt% Si Al joints. A slight difference in layer growth rate between the central and circumferential regions of the joint, with FT 2 and 7 s.	53

(continued)

Table 1. Continued.

WP materials	Parameters	Interlayer	Findings	Ref.
Al–Ti	D: 13 mm, FP: 50 MPa, FT: 2 s, RS: 1560 r/min, UP: 100 MPa, UT: 6 s	–	Critical IMC layer thickness: 5 μm. IMC layer thickness determines the joint characteristics.	54
Ti6Al4V–AA6061	D: 16 mm (Ti), D: 25 mm (Al), RS: 800, 1000, 1200 r/min, FP: 1.2 MPa, UP: 4 MPa, FT: 5–10 s, UT: 20 s, Zn coating layer thickness: 2 μm (800 r/min), 3 μm (1000 r/min), 5 μm (1200 r/min)	Electrodeposited Zn	Maximum TS: 189.92 MPa with an interlayer thickness of 0.5 mm, at RS: 1000 r/min.	55
Al–Ti	FP: 50 MPa, FT:2 s, UP: 100 MPa, UT: 6 s	–	Critical IMC thickness: 5 μm	56
AA6061/Ti6Al4V	RS: 1000 r/min, FP: 1 MPa,	–	Maximum weld interface temperature: 468.2°C reaches within 3.5 s.	57
cp Ti–cp Al	RS: 26–40 s^{-1}, FP: 50 MPa, FT: 1–2 s, UP: 50–150 MPa, UT: 6 s	–	Sound joint without fracture at weld interface produced up to 873K × 3.6 ks heat treatment with no IMC. Joint properties deteriorate at a longer heating time.	58

D: work diameter (mm); RS: rotational speed (r/min); cp: commercially pure; IMC: intermetallic compounds; FP: friction pressure; FT: friction time; UP: upset pressure; UT: upsetting time; JE: joint efficiency; TS: tensile strength.

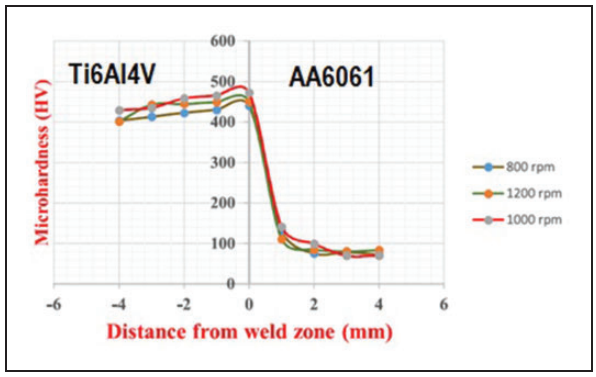

Figure 4. Effect of RS on microhardness of AA6061/Ti6Al4V joints.[2]

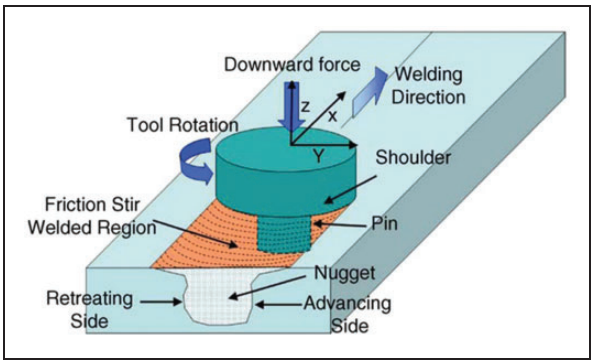

Figure 5. A schematic diagram of the friction stir welding process.[59]

the tool erosion and charring of the low melting point materials, the high melting point material is frequently kept on the advancing side (AS) and offsetting of the nonconsumable tool is towards the low melting point material from the interface of the butt joint. Furthermore, different coating methods on the tool are also suggested to avoid tool erosion caused by loss of surface quality and inclusions of fragments inside the weld.[70] Also, hybrid (GTAW-assisted) FSW process,[60] ultrasonic vibration-assisted FSW process[38] improve the life of the tool is also claimed.

Tool design and geometry. Tool design and its geometry affect the heat flow and material deformation, which resulted in microstructure and mechanical properties. The tool geometry influences the material mixing during welding. The important feature of tool design includes shoulder diameter, its surface characteristic, probe profile, its size, and its other characteristics of the surface.[71] According to Rostami et al.,[34] at zero tool probe offset (TPO), stir zone (SZ) grain size increase with an increase in HI. With similar HIs, the grain size produced using the cylindrical pin profile is larger than the conical square pin profile, which is attributed to material deformation and pulsating stirring action.

Tool rotational speed. TRS and WS influence the total HI. Choi et al.[13] claimed that the mechanical properties gradually improved with an increase of TRS from

Table 2. Summary of suggested parameters and findings of Al–Ti friction stir butt welds.

WP materials	Process	AS-RS	Thk	Interlayer	Tool design	Parameters	Findings	Ref.
Ti6Al4V-2024-T3 Ti6Al4V-7075-T651	FSW	Ti–Al	2 mm	–	TM: SKD61 850, SD: 20 mm, SPR: 2.5, PL: 1.9 mm, RD: 6 mm	TRS: 850 r/min, WS: 100, 200, 300 mm/min, TA: 3°, TPO: 0.5 mm on Ti side, VF: 7.8 kN	At WS: 300 mm/min TS: 311 MPa At WS: 300 mm/min TS: 201 MPa	3
Ti6Al4V-A6061-T6	FSW	Al–Ti	5 mm	–	TM: SKD61, SSP: Flat, SD: 15 mm, PSP: TCH, PD: 4.7 mm, SPR: 2.5, PL: 4.5 mm, RD: 6 mm, TD: 4 mm, ('L' shaped, modified joint)	TRS: 1000 r/min, WS: 150 mm/min, TA: 3°, TPO: 2 mm Al side	TS: 134 MPa with JE: 35% of Al	4
Pure Ti and pure Al	FSW	Ti–Al	2 mm	–	TM: WC-based alloy tool, SSP: Flat, SD: 12 mm, PSP: SC, SPR: 3, PL: 1.9 mm, RD: 4 mm	TRS: 500–1200 r/min, WS: 100 mm/min, TA: 3°, TPO: 0.1–0.2 mm on Ti side	At 1000 r/min–100 mm/min–0.1 mm defect-free welds with achieved with TS: 97 MPa with JE: 88% of Al	13
cp Al to cp Ti	FSW	Ti–Al	4 mm	–	TM: WC–8% Co, SSP: Flat, SD: 20 mm, PSP: SC, PD: 3.5 mm, SPR: 5, PL: 3.5 mm, RD: 4 mm	TRS: 800 r/min, WS: 40 mm/min, TPO: 2 mm on Al side	H: 170–218HV,TS: 117 MPa, EL: 25%	17
cp Al to cp Ti	FSW	Ti–Al	4 mm	200 μm Zn	TM: WC–8% Co, SSP: Flat, SD: 18 mm, PSP: SC, PD: 3.5 mm, SPR: 4.5, PL: 3.2 mm, RD: 4 mm	TRS: 900 r/min, WS: 90 mm/min, TA: 2.5°, TPO: 1.6 mm	The intermetallic phase thickness depends on particle size, local elemental composition, and temperature evolution during welding	18
cp Al to cp Ti	FSW	Ti–Al	4 mm	200 μm Nb	TM: WC–8% Co, SSP: Flat	TRS: 900 r/min, WS: 90 mm/min, TPO: 1.6 mm on Al side	EL: 34%, TS: 66 MPa, JE: 65% of Al	19
cp Al to cp Ti	FSW	Ti–Al	4 mm	200 μm Cu	TM: WC–8% Co, SSP: Flat, SD: 18 mm, PSP: SC, PD: 3.5 mm, SPR: 3.6, PL: 3.2 mm, RD: 5 mm	TRS: 800 r/min, WS: 90 mm/min, TPO: 1.7 mm, 2.1 mm, 2.5 mm on Al side	High hardness in the weld with TPO: 1.7 mm.	20
Ti6Al4V–A6061-T6	FSW	Ti–Al	2 mm	–	TM: WC–Co, SSP: Concave, SD: 15 mm, PSP: SC, SPR: 2.5, PL: 1.9 mm, RD: 6 mm	TRS: 750–1000 r/min, WS: 120 mm/min, TA: 3°, TPO: 0 mm, 0.3 mm, 0.6 mm, 0.9 mm, 1.2 mm on Al side, VF: 7.5 kN	At 750 r/min–0.9 mm, TS: 192 MPa; At 750 r/min–1.2 mm, TS: 193 MPa; At 1000 r/min–0.9 mm, TS: 197 MPa with JE: 62% of Al	21
Ti6Al4V–A6061-T6	FSW	Ti–Al	2 mm	–	TM: WC–Co, SSP: Concave, SD: 15 mm, PSP: SC, SPR: 2.5, PL: 1.9 mm, RD: 6 mm	TRS: 500, 750, 1000, 1250 r/min, WS: 120, 160, 200, 280 mm/min, TA: 3°, TPO: 0 mm, 0.3 mm, 0.6 mm, 0.9	Created process window for following conditions 750 r/min–200 mm/min–0.6 mm; 750 r/min–120 mm/min–	22

(continued)

Table 2. Continued.

WP materials	Process	AS-RS	Thk	Interlayer	Tool design	Parameters	Findings	Ref.
						mm, 1.2 mm on Ti side, VF: 7.5 kN	0.9 mm; 750 r/min–160 mm/min–0.9 mm; 750 r/min–280 mm/min–0.9 mm; 750 r/min–280 mm/min–0.9 mm; 750 r/min–120 mm/min–1.2 mm; 750 r/min–160 mm/min–1.2 mm; 750 r/min–200 mm/min–1.2 mm; 500 r/min–160 mm/min–1.2 mm; 500 r/min–200 mm/min–1.2 mm to get defect free welds At 750 r/min–200 mm/min–1.2 mm, TS: 215 MPa with JE: 68% of Al	
Ti6Al4V–Al–6Mg	FSW	Ti–Al	2 mm and 4 mm	–	TM: WC–13 wt% Co, SSP: Flat, SD: 15 mm, PSP: TC, PD: 2.4 mm, SPR: 2.5, PL: 2.2 mm, RD: 6 mm, TD: 4	TRS: 1200, 1800, 2400 r/min, WS: 60 mm/min, TA: 0°, TPO: 0.5, 1, 1.5, 2 mm on Al side	Created process window for following conditions: 1200 r/min–60 mm/min–0.5 mm; 1800 r/min–60 mm/min–0.5 mm with ∼10 μm interlayer thk and JE: 84% of Al; 1200 r/min–60 mm/min–1 mm with ∼2 μm interlayer thk and TS: 292 MPa, JE: 92.65% of Al; 1800 r/min–60 mm/min–1 mm with JE: 92.65% of Al; 1200 r/min–60 mm/min–1.5 mm with ∼10 μm interlayer thk; 1200 r/min–60 mm/min–0.5 mm	23
cp Al to cp Ti	FSW	Ti–Al	4 mm	200 μm Zn	TM: WC–8% Co, SSP: Flat, SD: 18 mm, PSP: SC, PD: 3.5 mm, SPR: 4.5, PL: 3.2 mm, RD: 4 mm	TRS: 900 r/min, WS: 90 mm/min, TA: 2.5°, TPO: 1.6 mm on Al side	H: ∼200HVN,TS: 138 MPa, EL: 48%	24
Ti6Al4V–AA2024-T3	FSW	Ti–Al	4 mm	–	TM: WC–8% Co, SSP: Flat, SD: 20 mm, PSP: SC, PD: 3.5 mm, SPR: 5, PL: 3.2 mm, RD: 4 mm	TRS: 800 r/min, WS: 40 mm/min, TPO: 2 mm on Al side	For 2nd pass UTS: 271 ± 6 MPa, El: 9 ± 1.0 %, JE: 60% For 1st pass UTS: 231 ± 6 MPa, El: 7.4 ± 0.3 %, JE: 50%	25

(continued)

Table 2. Continued.

WP materials	Process	AS-RS	Thk	Interlayer	Tool design	Parameters	Findings	Ref.
Ti6Al4V–AA5052-H32	FSW	Ti–Al	2 mm	–	TM: WC–Co, SSP: Flat, SD: 16 mm, PSP: SC, SPR: 2.67, PL: 1.9 mm, RD: 6 mm TM: WC–Co, SD: 16 mm, PSP: TSQ, SPR: 2.67, PL: 1.9 mm, RD: 6 mm	TRS: 500, 710, 1000 r/min, WS: 40, 80 mm/min, TA: 2°, TPO: 0, 0.5, 1 mm on Ti side	Created process window for following conditions 500 r/min–40 mm/min–0.5 mm; 710 r/min–40 mm/min–0.5 mm; 1000 r/min–80 mm/min–0.5 mm to get defect-free welds using TSQ tool. At 500 r/min–40 mm/min–0.5 mm with JE: 94% of Al	34
Ti6Al4V–5A06 Al	FSW	Ti–Al	2 mm and 4 mm	–	TM: YG12, WC–12 wt% Co, SD: 15 mm, PSP: Concave, PD: 2.4 mm, SPR: 2.5, PL: 2.2 mm, RD: 6 mm, TD: 4, ("L" shaped, modified joint)	TRS: 1200 r/min, WS: 60 mm/min, TPO: 0.5 mm on Al side	TS: 265 MPa with JE: 84.13% of Al	41
TiAl6V4–2024-T3	FSW	Ti-Al	2 mm	–	TM: standard tool steel with coated shoulder and pin, PSP: TCH, SD: 18 mm, SPR: 3, RD: 6 mm	TRS: 800 r/min, WS: 80 mm/min	TS: 348 ± 7.67 MPa with JE: 73% of Al	42
Pure Ti and AA6061-T651	FSW	Ti–Al	4 mm	–	TM: WC–12% Co, SSP: Flat, SD: 18 mm, PSP: TC, SPR: 3, PL: 3.8 mm, RD: 4 mm, TD: 4 mm	TRS: 1070 r/min, WS: 20 mm/min, TA: 2°, TPO: 2 mm on Al side	EL: 3.6 %, TS: 120MPa, JE: 42% of Al using water cooling	60
cp Al to cp Ti	FSW	Ti–Al	4 mm	200 μm Zn	TM: WC–8% Co, SSP: Flat, SD: 18 mm, PSP: SC, PD: 3.5 mm, SPR: 4.5, PL: 3.2 mm, RD: 4 mm	TRS: 900 r/min, WS: 90 mm/min, TPO: 1.2 mm,1.6 mm, 2.2 mm, 4 mm on Al side	TS: 132 MPa, EL: 50% at TPO: 1.6 mm	61
TC1 Ti alloy – LF6 Al	FSW	Ti–Al	2 mm	–	SD: 15 mm, SSP: Concave, PSP: TCH, SPR: 3, PL: 1.85 mm, RD: 5 mm	TRS: 600–1180 r/min, WS: 95–190 mm/min, TPO: 2 mm	At TRS: 950 r/min, WS: 118 mm/min TS: 131.1 MPa	62
	FSLW	Al–Ti	Al on top of Ti	–	SD: 15 mm, SSP: Concave, PSP: TCH, SPR: 3.75, PL: 2.1 mm, RD: 4 mm	TPO: 0.5 mm	At TRS: 1500 r/min, WS: 60 mm/min, Shear strength: 48 MPa	
Al6061-Ti	FSW	Ti–Al	4 mm	–	TM: WC, PSP: TC, SD: 18 mm, SPR: 3, PL: 3.8 mm, RD: 6 mm, TD: 4 mm	TRS: 765, 1070, 1500 r/min, WS: 20, 31.5, 50 mm/min, TA: 1°, 2°, 3°, TPO: 2 mm	At TRS: 1500 r/min, WS: 60 mm/min, TPO: 1 mm, UTS: 142.97 MPa, YS: 59.48 MPa, JE: 9.82%	63
cp Ti–5083 H-321	FSW	Ti–Al	3 mm	–	PSP: TC	TRS: 1120 r/min, WS: 50 mm/min	H: 480 Vickers	64

(continued)

Table 2. Continued.

WP materials	Process	AS-RS	Thk	Interlayer	Tool design	Parameters	Findings	Ref.
Ti-4%Al-Al-1%Si	FSW	Ti–Al	5 mm	–	TM: HSS, SD: 20 mm, PSP: SC, PD: 4.2 mm, SPR: 5, RD: 6 mm (intercalated butt joint)	TRS: 1100 r/min, WS: 5 mm/min	Joints made indicate a weak joint	[65]
cp Ti-7075	FSW	Ti–Al	3 mm	–	SD: 20 mm, SSP: Concave, PSP: TC, SPR: 3.33, PL: 2.6 mm, RD: 6 mm, TD: 3	TRS: 1120 r/min, WS: 50 mm/min	H: 360 HV10	[66]
Ti6Al4V–A6061-T6	FSW	Ti–Al	2 mm	–	TM: WC–Co-based alloy, SD: 15 mm, SSP: Concave, PSP: SC, PL: 1.9 mm, RD: 6 mm (intercalated butt joint), VF: 7.5 kN	TRS: 500,750, 1000,1250 r/min, WS: 120,160,200,280 mm/min, TA: 3°, TPO: 0, 0.3, 0.6, 0.9, 1.2 mm Ti side	At low TRS and higher WS wormhole defects were produced in the stir zone of Al. The more TPO, the higher WS, and TRS produced defects in Ti alloy. At smaller TPO, lower TRS, and higher WS, no bonded defect at the bottom	[67]

cp: commercially pure; TM: tool material; SSP: shoulder surface profile; SD: shoulder diameter (mm); PSP: probe surface profile; TC: taper cylindrical or conical; TCH: threaded conical; SC: cylindrical; TSQ: Taper square; PD: plunge depth (mm); PL: probe length (mm); RD: root diameter (mm); TD: tip diameter (mm); SPR: shoulder-to-probe diameter ratio; TRS: tool rotational speed (r/min); WS: weld speed (mm/min); TA: tool tilt angle (°); VF: vertical force; TPO: tool probe offset; thk: thickness (mm); JE: joint efficiency; EL: elongation (%); H: hardness; TS: tensile strength; UTS: ultimate tensile strength; YS: yield strength.

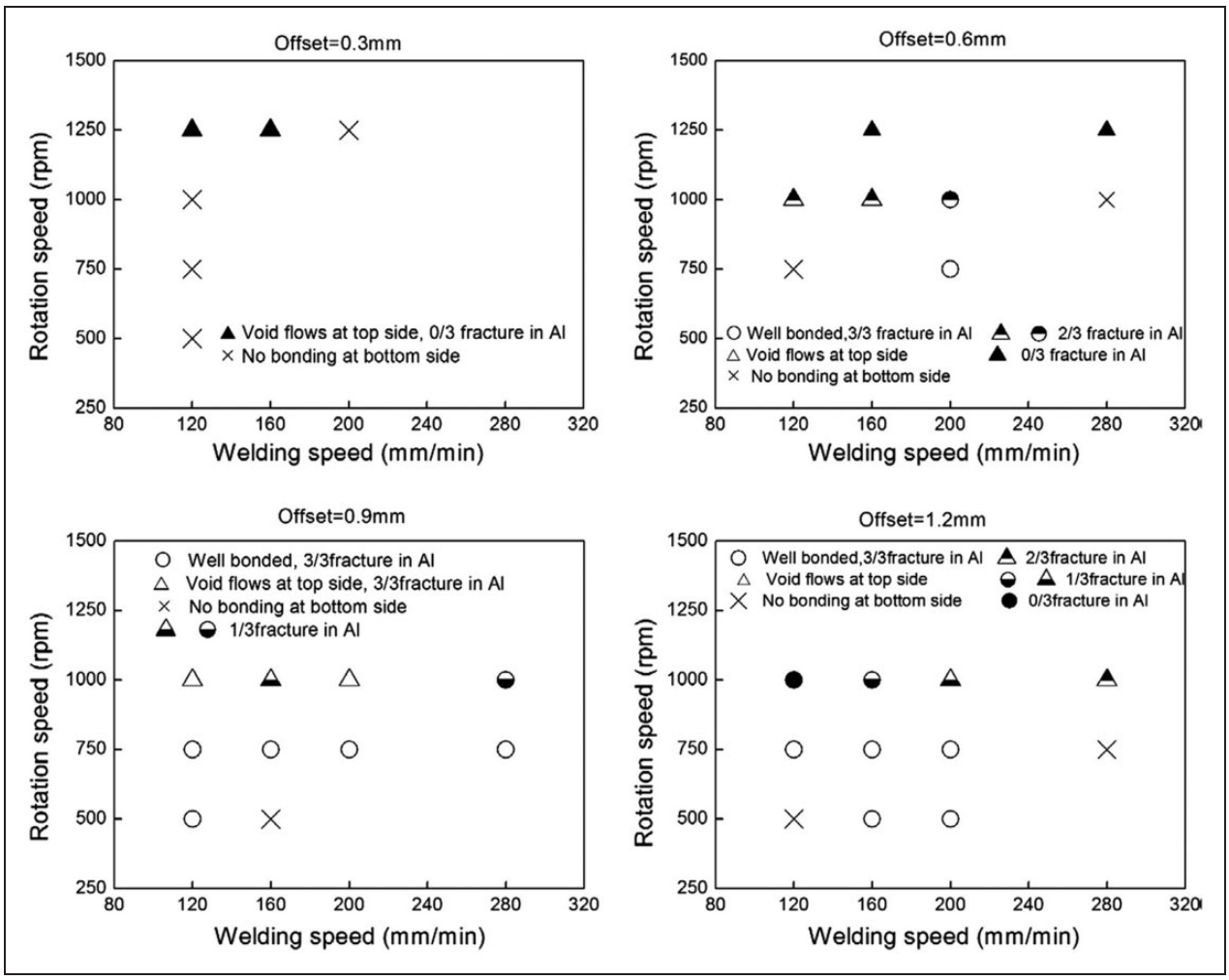

Figure 6. Process parameter window for sound joints with different TPOs: (a) 0.3 mm, (b) 0.6 mm, (c) 0.9 mm, and (d) 1.2 mm.[22]

500 to 800 r/min by keeping other parameters like TPO and WS constant, while it is reduced with an additional increase of TRS from 800 to 900 r/min. A similar kind of observation was claimed by Zhang et al.[41] According to Song et al.[21] at constant TRS: 750 r/min, TS increases marginally with an increase in TPO. On the contrary, at constant TRS: 1000 r/min, TS increases slightly by an increase in TPO. Wu et al.[22] studied that at TRS: 500 r/min, WS: 160 mm/min, TPO: 1.2 mm, a well-bonded thin interfacial layer formed and joint failed in the Al alloy SZ, whereas at TRS: 750 r/min WS: 200, 120, 280 mm/min, TPO: 1.2, 0.9 mm, soundly bonded interface with no thick mix and reaction layer formed and joint failed TMAZ/HAZ of Al alloy as shown in Figures 6 and 7. However, at TRS: 1000 r/min, WS: 120 mm/min, TPO: 1.2 mm, a thick interface formed. Rostami et al.[34] ascertained that using the TSQ tool, at TRS of 500, 710, and 1000 r/min and WS of 40 and 80 mm/min defect-free joints were achieved respectively.

Weld speed. The ratio of TRS/WS was studied by Rostami et al.[34] for Ti6Al4V and AA5052 welds with TPO: 0.5 mm, keeping this ratio constant as 12.5 r/min for TRS of 500 and 1000 r/min, and WS of 40 and 80 mm/min, respectively. It is observed that the SZ grain size for these parameters was different. The study shows that this rule is not valid for the FSW of dissimilar weld materials. According to the results of Wu et al.,[22] it is seen from Figure 6 that at constant TRS: 750 r/min and TPO: 1.2 mm, the tensile strength linearly varying with WS, a similar trend was observed at constant TRS: 1000 r/min and TPO: 0.6 mm. However, the trend is different for other conditions. Chen et al.[62] claimed that for joining TC1 Ti and LF6 Al alloys with FSW at constant TRS: 750 r/min with WS: 118 and 150 mm/min, no sufficiently stirring and mixing in the SZ resulted in the crack at the interface and poor tensile strength. On the contrary, at constant TRS: 950 r/min with WS increased from 118 to 150 mm/min, more IMC formed causing a decrease in tensile strength, and at 118 mm/min maximum TS: 131 MPa achieved in butt configuration. They extended their studies in lap configuration at different HIs. At constant TRS: 1500 and WS varied from 60, 118, 150 mm/min, it has been observed that maximum shear strength of 48 MPa achieved at WS: 60 mm/min, whereas at

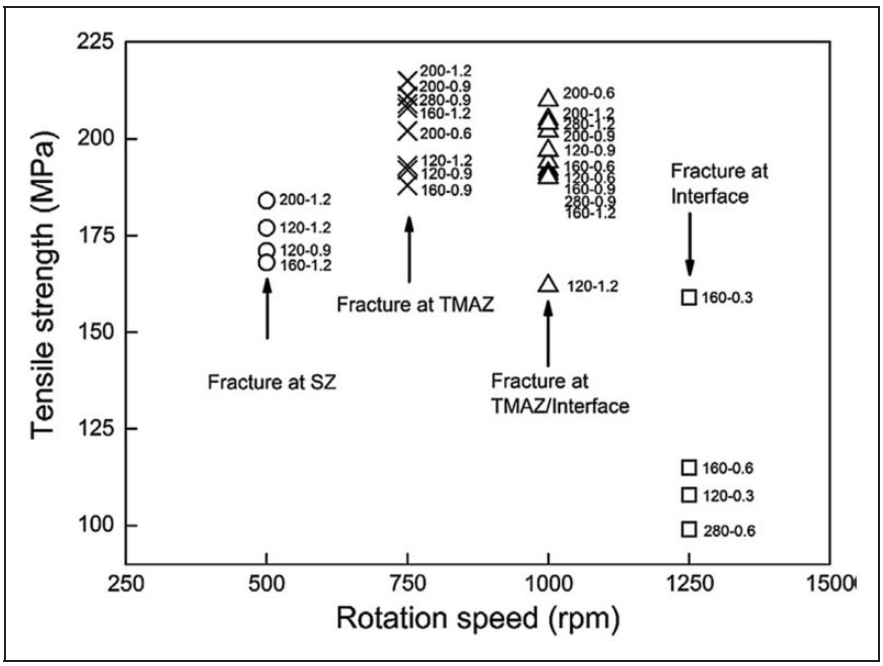

Figure 7. Effects of the process parameters on the tensile strength of Al–Ti joints.[22]
SZ: stir zone; TMAZ: thermomechanically affected zone.

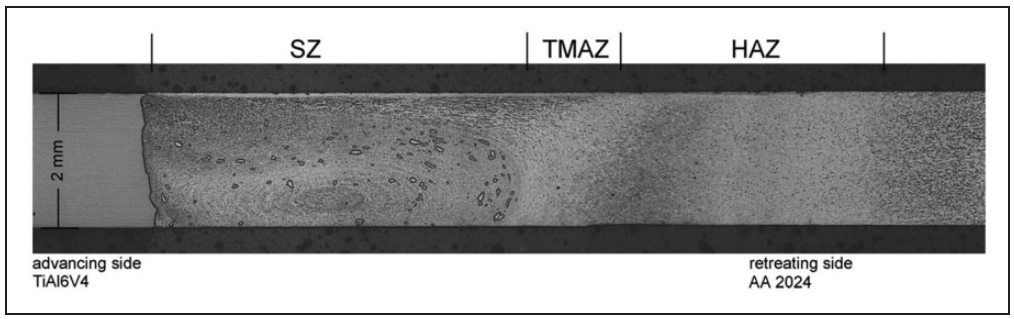

Figure 8. Macrograph of TiAl6V4 and AA2024-T3 FSWed joint.[42]
SZ: stir zone; TMAZ: thermomechanically affected zone; HAZ: heat-affected zone.

WS: 150 mm/min shear strength of 0 MPa was attained. Increasing WS from 100 to 200 mm/min, a small increase in the joint tensile strength achieved but further increase in WS up to 300 mm/min, sudden growth in the tensile strength was seen for Ti-2024, Ti-7075, Ti6Al4V-2024, and Ti6Al4V-7075. Patel et al.[63] employed Taguchi's grey relational analysis to optimize the process parameters. However, the effect of these parameters was not discussed.

Tool probe offset. It is recommended that the higher melting temperature work material should be placed on the AS with the TPO from the interface of the butt joint towards the low melting point temperature work material in butt joint configuration to avoid tool erosion and charring of the low melting point materials,[71] which support most of the literature.[12,14–16,24–27,31,33,35,36] The TPO plays a crucial role in the Ti fragments formation than the TRS. The quantity of Ti fragments reduced with the reducing TPO from 0.2 to 0.1 mm.[13] At 0.1 mm TPO, TS increases with an increase in TRS from 900 to 1000 r/min then decreases with up to 1200 r/min when TPO is into the pure Ti side. A similar observation was suggested when at TRS: 750 r/min, WS: 200 mm/min with TPO: 1.2 mm as shown in Figure 8 and when TPO is into the Al side.[21]

Li et al.[23] claimed that as TPO is increased by keeping other process parameters like TRS and WS constant with modified butt joint, the thickness of the diffusion interlayer is ~2 μm at TPO from 0.5 to 1.0 mm. However, the interlayer thickness less than 10 μm with a mixed band-like structure was formed at TPO 1.5 mm. Buffa et al.[72] analyzed the complex flow of the material in dissimilar FSW of AA2024–Ti6Al4V butt and lap joints using the implicit Lagrangian code DEFORM-3D. Their results showed that TPO towards the Al side resulted in a more effective flow of the material behind the tool with improved material mixing.

Interlayer. It is claimed that during the welding of Al and Ti, the brittle intermetallic formation can be controlled using an interlayer and their selection should promote the ductile phase formation than brittle Ti–Al IMCs.[24] Kar et al.[24,25]studied the effect of the Zn interlayer on the FSW of cp Al–Ti alloys. It is observed that the Zn integrates with Al–Ti changes the phase growth and controls the Al_3Ti IMC phase structure. The Zn existence integrates elemental scattering and restricts the formation of brittle intermetallic phase, with significant progress in the weld tensile properties. Further, they[61] extended their work with different tool offsets and ascertained that the tool offset position is a key parameter for restricting the number of ternary materials mechanical mixing. In their similar work,[18] it is claimed that the mechanical stirring and thermal cycle promote the brittle intermetallic phase formation. In their other work,[19] the effect of Nb interlayer on FSW of cp Al–Ti alloys was investigated. It is revealed that the formation of intermetallics is restricted due to the presence of Nb as an interlayer with reduced tensile strength but higher ductility in comparison with parent Al alloy because of the defect formation in the weld zone due to the presence of Nb flakes. In their other work,[20] the influence of TPO with Cu interlayer in FSW of cp Al to cp Ti alloy was investigated. It is claimed that with higher tool offsets, root defects are formed, whereas the tool offset with less than the optimum value, wormhole defects are formed with the evolution of IMCs in the weld. The tool offset is a very important parameter, as hardness distribution varies with it. The large spread in weld hardness with lower values of tool offset.

Microstructure. According to Dressler et al.,[42] the macrostructure of TiAl6V4 and AA2024-T3 FSWed joints, an onion ring-shaped structure can be seen at the SZ as shown in Figure 8 where the TMAZ and HAZ are present on RS and these regions are absent on AS. The thickness of brittle Ti_xAl_x phases (possibly $TiAl_2$) found to be maximum 1 μm and swirl-like structure areas has the highest bond strength. According to Aonuma and Nakata,[3] the increase in WS decreases the HI, and hence, the narrow IMC phase is produced. At WS: 300 mm/min, flaws were seen in the vicinity of the groove in the Ti6Al4V-7075 joints. Further, only Ti and Al phases were found in the fractured surface of Ti-Al2024 and Ti6Al4V-Al joints. However, mainly Al, Ti, and Al_3Ti phases formed on the fractured surface of Ti–Al joints.

The effect of different TRSs was observed by Choi et al.[13] for pure Al–Ti FSW joints and revealed that at 700 r/min layer formed and at 800 r/min TiAl and Al_3Ti IMC layer formed while at 900 r/min $AlTi_3$, TiAl, and Al_3Ti IMC layer formed. It can be seen from Figure 9 that for all the TRSs, the initial Al_3Ti IMC layer was created at the interface of weld because of the least free energy of formation. By increasing the TRS from 800 to 900 r/min, defects formed near the weld interface due to more number of Ti fragments, which reduces the tensile strength. It was claimed that TPO is an important parameter in the Ti fragments formation than the TRS, whereby decreasing TPO from 0.2 to 0.1 mm, the amount of Ti fragments decreases.

Rostami et al.[34] explained the influence of the design of the tool pin and TPO on the microhardness profile of Ti6Al4V/AA5052-H32 alloy joints. It is claimed that defect-free joints were obtained with the hardness in SZ using the cylindrical tool pin is lesser than the TSQ tool. A sudden drop in hardness is observed at Al–Ti alloy interface with fractured surface showing Al_3Ti IMC formation and SZ hardness is not constant and the same is explained in Aonuma and Nakata[3] and Song et al.[21] However, Ghogheri et al.[64] achieved the highest SZ hardness 16 and 60% for cp Ti and Al 5083 alloy respectively, and the same is explained in Ghogheri et al.[66]

Zhang et al.[41] employed a modified L-type shape butt joint configuration for FSW of Al–Ti alloy using different process conditions as shown in Figure 10. It can be seen that most parts of the SZ consist of vortex flow (I and II) structure, which is similar to classical onion-ring morphology. Along with these, turbulent flow and hook structure with Ti particles were also seen in the SZ. It was observed insufficient or too large pin plunge value produces a lack of penetration defects at the root position in conventional FSWed joints. Further, if Al alloy is placed at the bottom side gives rise to irregular plastic flow of the material and produces voids and grooves. The occurrences of such defects are prevented with modified L-type shape joint configuration with successful Al/Ti bonding. It is claimed that high-quality joints are achieved using this modified joint configuration applied for different sheet thickness, which resulted in less tool pin and shoulder erosion, elimination of butt root flaws, and Al melting. The Ti–Al diffusion interlayer (2 μm thickness) is beneficial in terms of joint strength than the Ti–Al reaction interface structure (10 μm thickness) with bulky or continuous IMC interlayer.

Recently, Pereira et al.[73] investigated the nanocrystalline film, which serves as an interface bonding in Ti–Al alloys of FSWed joints using the spindle power control method to decrease the HI at the joint (~0.5 kJ/mm) as shown in Figure 11. The spindle power control mode is based on the thermal balance (steady-state HI) in the SZ where the spindle power is correlated with the torque and rotation speed. In the case of conventional control, the temperature changes throughout the process at constant speeds. It is observed that Al_3Ti IMC precipitates of nanometric sizes (<100 nm) as can be seen in Figure 12 improves the joint performance.

To summarize, for maximum tensile strength of dissimilar FSbWed joints of Al–Ti alloys, it is recommended that a minimum of ~2 μm the IMC thickness

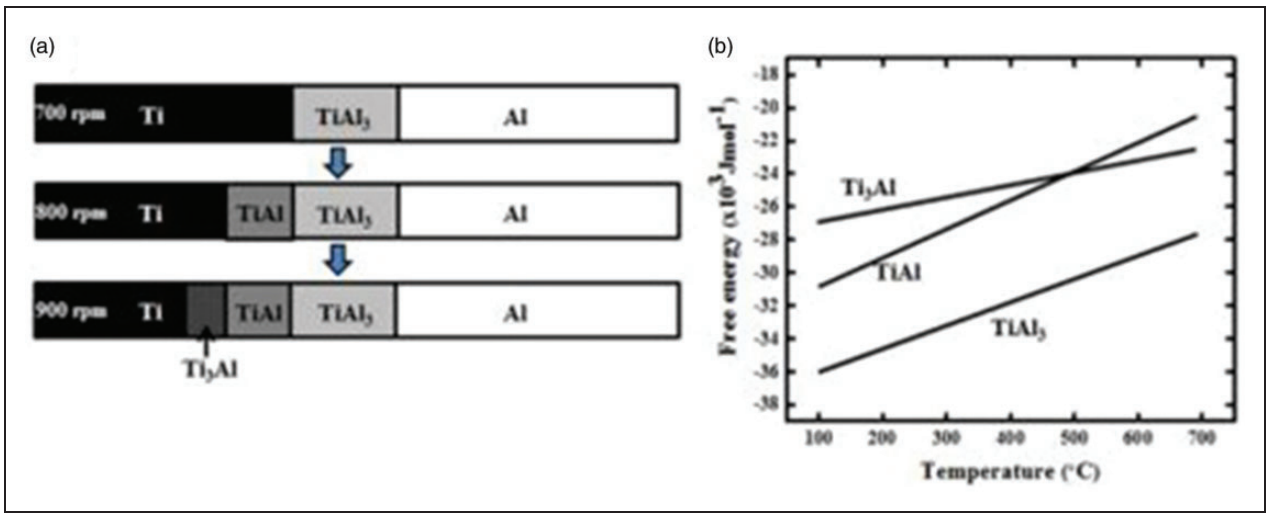

Figure 9. The schematic diagram of the (a) intermetallic layers formation at different TRSs and (b) the free energies of Ti-Al IMCs at various temperatures.[13]

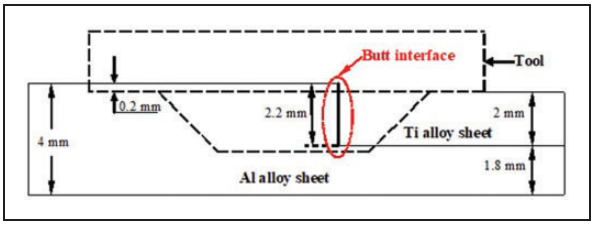

Figure 10. Modified L-type shape joint configuration for FSW of Al–Ti alloy.[41]

is suitable. FSbW of Al–Ti alloys showed a minimum tensile strength of 66 MPa using Nb interlayer while the maximum tensile strength of 300 MPa using gas tungsten arc welding-assisted friction stir welding (GTAWaFSW). The hybrid FSW approaches like ultrasonic-assisted FSW (UaFSW) and GTAWaFSW revealed much of the improvement in the joint tensile strength. As of now, very few interlayer materials (Zn, Nb, Cu) with or without offset has been studied, there is a need to explore other interlayer material that finds good compatibility with the Al–Ti system. Further, the studies on different thicknesses of interlayer material with or without offset can be explored. TPO has a strong influence on the interfacial microstructures and mechanical properties of the joints. It is recommended to keep TPO on the Al side to get sound joints. The higher values of TPO give root defects whereas TPO less than the optimum value, yields wormhole defects with the evolution of IMCs in the weld. Similarly, the TRS and WS influence the total HI and the microstructure of the joint. The ratio of TRS/WS (ω/υ) shows direct relation in the SZ grain size with zero TPO. However, this rule is not valid when an increase in TPO. To get maximum mechanical properties, it is recommended to control the TPO, TRS, and WS. This can be achieved by process optimization using the design of experiments, process simulation, or machine learning approaches to get a good balance of the weld properties. Most of the published works considered TA of 3°. However, the effect of TA on the microstructure and mechanical properties of FSbW of Al–Ti alloys can be explored.

Friction stir lap welding

As explained in the previous section, FSLW is a kind of the FSW process, wherein the workpieces to be welded are held in lap position as depicted in Figure 13. Similar to FSbW, the lower melting temperature work material is placed on top of the higher melting temperature work material. If the placement of the changes, then it affects the weldability and tool wear.[71] The process parameters, which are affecting the joint performance, are TRS, WS, VF, and tilt angle (TA) that have been shown in Table 3. These parameters are explained in detail for the Al–Ti weld using FSLW.

Tool rotational speed. TRS and WS both have a major influence on the maximum temperature, which is directly proportional to the pseudo-heat index (ω^2/υ), where TRS (ω, r/min) and WS (υ, r/min).[5,59] The hardness distribution across the Al–Ti joint is significantly affected by HI. Yue et al.[80] performed FSW of Al–Ti joints at different TRSs of 1200, 800, 500, and 300 r/min and constant WS of 30 mm/min using the W-25Re tool. It is claimed that the void defect was observed at high TRS at the joint interface. The size of the void decreases with decreasing the TRS. At 300 r/min defect-free joints were obtained. It is claimed that the hook acts as a lock during shear testing. The opposite forces prevent the relative movements of the sheets. The effective sheet thickness is the

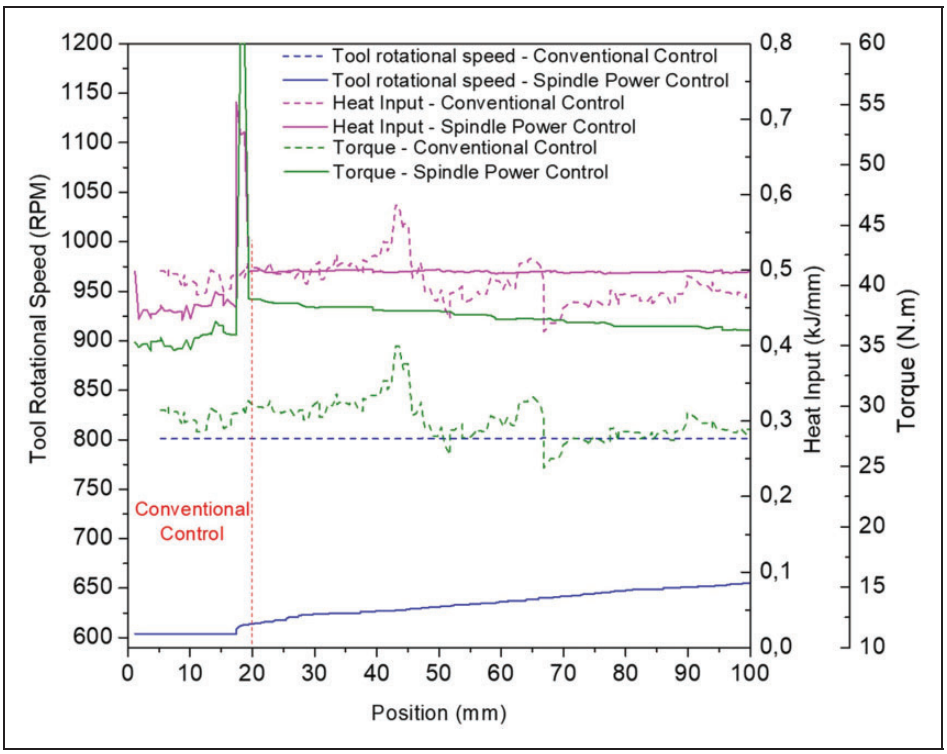

Figure 11. Comparison of FSW variables in conventional and spindle power control modes for heat input: ~0.5 kJ/mm.[73]

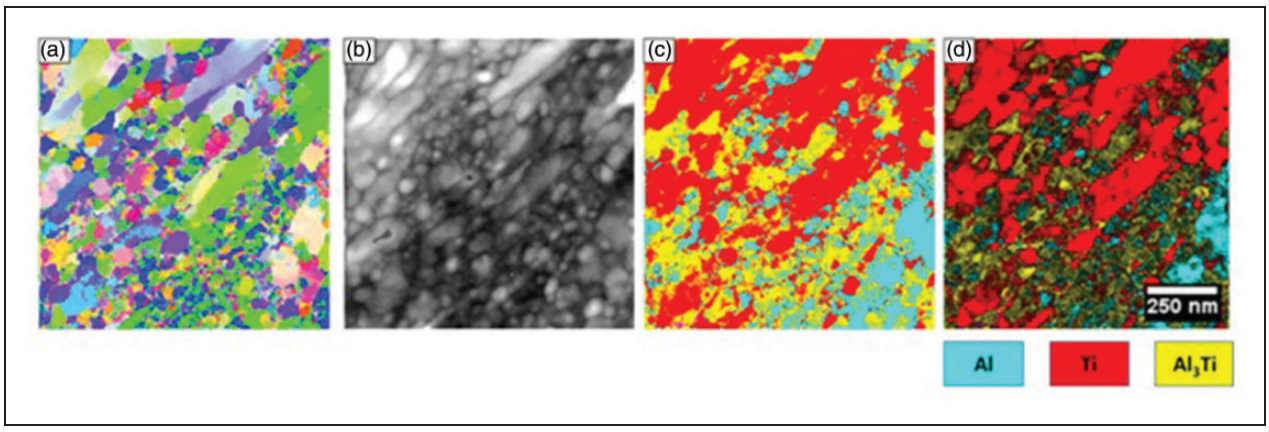

Figure 12. (a) Precession electron diffraction crystallography orientation map, (b) correlation index, (c) phase index, and (d) reliability index + phase mapping indicating nanometric size precipitates of Al_3Ti IMC.[73]

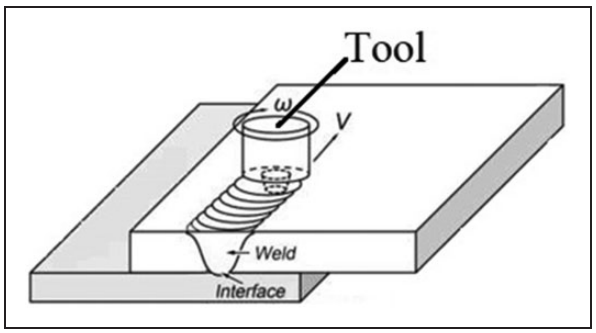

Figure 13. A schematic diagram of friction stir lap welding.

distance from the top of the sheet to the hook which governs the load-bearing area. Smaller effective sheet thickness poor joint mechanical properties and vice versa have been reported.[80] It is also reported that behind the hook there is a lack of bonding that reduces the joint mechanical properties. Yu et al.[5] revealed that a maximum strength was achieved at TRS of 1000 r/min and WS of 100 mm/min. However, with an additional rise in HI the strength decreases. The effect of HI on the joint interface evolution is shown in Figure 14. At TRS less than 1000 r/min defect-free joints, while greater than 1000 r/min,

Table 3. Summary of suggested parameters and findings of Al–Ti friction stir lap welds.

WP materials	Top–bottom	Thk	Tool design	Parameters	Findings	Ref
AA6061-T6–Ti6Al4V	Al on top of Ti at RS	Al: 3 mm Ti: 2 mm	TM: W-25Re, SSP: Concave, SD: 12 mm, PSP: TC, PD: 0.1 mm, SPR: 4, PL: 3.1 mm, RD: 3 mm	TRS: 600–1400 r/min, WS: 60–140 mm/min, TA: 3°, TPO: 0.1–0.2 mm on Ti side	At TRS: 1000 r/min, WS: 100 mm/min, with SS: 147 MPa	5
ADC12 cast Al–pure Ti	Al on top of Ti	Al: 4 mm Ti: 2 mm	TM: WC–Co, SD: 15 mm, PSP: SC, PL: 3.9 mm, RD: 5 mm	TRS: 1500 r/min, WS: 60, 90, 120 mm/min, TA: 3°, VF: 5.39 kN	Maximum failure load: 9.39 kN (62% of Al), WS: 90 mm/min	6
Pure Al–Ti6Al4V (multi-pass)	Al on top of Ti	Al: 2 mm Ti: 3 mm	TM: Inconel 718 (shoulder) and WC–13 wt% Co (cutting pin), SD: 15 mm, SSP: Flat, PSP: rotary burrs with spiral cutting-edges, PL: 2 mm, RD: 6 mm	TRS: 1200 r/min, WS: 60 mm/min	Interval banding structure with ~50 μm interlayer is produced. Good anti-oxidation performance of the specimen is exhibited at 650 °C in the air	7
Pure Al–Ti6Al4V (multi-pass)	Al on top of Ti	Al: 2 mm Ti: 3 mm	TM: H13 steel (holder with fix screws), Inconel 718 (shoulder) and WC–13 wt % Co (cutting pin), SD: 15 mm, SSP: Flat, PSP: rotary burrs with 15 spiral cutting-edges, PL: 2 mm, RD: 6 mm	TRS: 1200 r/min, WS: 60 mm/min	At 500°C, Maximum failure load: ~8.5 kN, EL: ~2.5%	8
AA6061–Ti6Al4V	Al on top of Ti	Al: 3 mm Ti: 2 mm	TM: W-25Re, SSP: Concave, SD: 12 mm, PD: 0.1 mm PL: 3.1 mm, RD: 3 mm	TRS: 800,1000, 1200 r/min, WS: 60, 100, 140 mm/min, TA: 3°	Maximum failure load: 4500 N with a 7.5 μm interface At TRS: 1000 r/min, WS: 100 mm/min	31
AA6061–Ti6Al4V	Al on top of Ti at RS	Al: 3 mm Ti: 2 mm	PL: 2.9, 3.1, 3.3 mm, SD: 12 mm, RD: 4.1 mm, TD: 2.9, 3.0, 3.1 mm PD: 0.1 mm, semi-cone angle of 10°	TRS: 1000 r/min, WS: 100 mm/min, TA: 3°	At PL: 3.1, SS: 147.5 MPa, EL: 4.1%	35
Ti6Al4V–AA2024-T4	Ti on top of Al	Al: 1.2 mm Ti: 1.6 mm	TM: W-25Re, SSP: Flat, SD: 13 mm, PSP: TC, PD: 2.6 mm PL: 2.4 mm, RD: 4.5 mm, semi-cone angle of 30°	TRS: 900,1200,1500 r/min, WS: 50, 100, 200 mm/min, TA: 2°	Maximum failure load: 200 N/mm At TRS: 900 r/min, WS: 200 mm/min, H: up to 360–370 HV	74
AA1060–Ti6Al4V	Al on top of Ti at RS	Al: 3 mm Ti: 3 mm	TM: WC, SSP: Concave, SD: 25 mm, PD: 3.2 mm, PL: 3.1 mm, RD: 3 mm	TRS: 950 r/min, WS: 150, 235, 300, 375, 475 mm/min, TA: 0°	Maximum failure load: 1910 N (~Al = 1853 N) At WS: 300 mm/min	75
TC1-LF6 Al	Al on top of Ti at AS	Al: 2 mm Ti: 2 mm				76

(continued)

Table 3. Continued.

WP materials	Top–bottom	Thk	Tool design	Parameters	Findings	Ref
			SSP: Concave, PSP: TCH, SD: 15 mm, PL: 2.1 mm, RD: 4 mm	TRS: 600, 900, 1500 r/min, WS: 60, 95, 118, 150 mm/min, TA: 2°	Maximum failure load: 2.8 kN, H: 502 HV, TRS: 1500 r/min, WS: 60 mm/min	
AA2024-T4–AA7475-T6 (top butt) and Ti6Al4V (bottom)	AA2024-T4–AA7475-T6	Al: 4 mm Ti: 2 mm	TM: H13 steel, SD: 20 mm, PSP: TC, PL: 4 mm, RD: 6 mm, TD: 5 mm	TRS: 1100, 1300, 1500 r/min, WS: 20, 30, 40 mm/min, TA: 1°, 2°, 3°	TA: 1° gives high penetration in the Al plate. VF showed that WS and TA exert greater influence	77
AA6060-T5–Ti-6Al-4V	Al on top of Ti	Al: 6 mm Ti: 2.5 mm	TM: H13 tool steel, SD: 25 mm, PSP: threaded, RD: 6 mm	TRS: 1400 r/min, WS: 20, 80 mm/min, TA: 2.5°, VF: 5.39 kN	The low growth rate of thin interface layer formed at zero penetration depth has higher fracture toughness than Al–Fe intermetallics	78
AA6061–Ti6Al4V	Al on top of Ti	Al: 3 mm Ti: 2 mm	TM: W-5Re, SD: 12 mm, PSP: TC, TD: 3 mm, PL: 3.13 mm	TRS: 1000 r/min, WS: 40, 80, 120, 160 mm/min, TA: 3°	Maximum failure load: 4026 N at WS: 80 mm/min	79
AA6061-T6–Ti6Al4V	Al on top of Ti	Al: 2.7 mm Ti: 2.5 mm	TM: W-25Re, SD: 15 mm, SSP: Concave, PSP: TC, RD: 7 mm, TD: 4 mm	TRS: 300, 500, 800, 1200 r/min, WS: 30 mm/min, TA: 2.5°.	The defect-free joint can be obtained at TRS: 300 r/min	80

cp: commercially pure; TM: tool material; SSP: shoulder surface profile; SD: shoulder diameter (mm); PSP: probe surface profile; TC: taper cylindrical or conical; TCH: threaded conical; SC: cylindrical; PD: plunge depth (mm); PL: probe length (mm); RD: root diameter (mm); TD: tip diameter (mm); SPR: shoulder-to-probe diameter ratio; TRS: tool rotational speed (r/min); WS: weld speed (mm/min); TA: tool tilt angle (°); VF: vertical force; TPO: tool probe offset; thk: thickness (mm); EL: elongation (%); H: hardness; SS: shear strength.

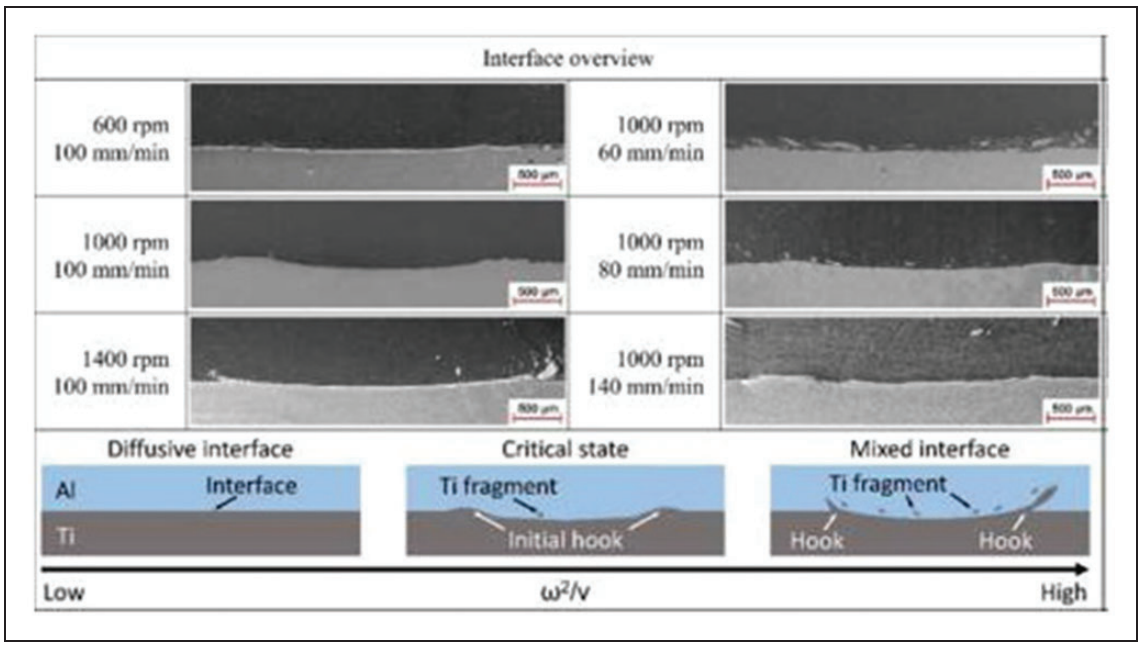

Figure 14. Effect of heat input on the evolution of the joint interface.[5]

surface flashes, and hooks within the joint were obtained. On the other hand, at constant TRS of 1000 r/min, with varying WS 60–80 mm/min flashes and hooks observed, while WS greater than 100 mm/min flashes and hooks hardly seen. Furthermore, initially, Al_3Ti was generated at the Al–Ti interface while, TiAl formed at the Ti and Al_3Ti interface, via the Al diffusion across the Al_3Ti layer. In their other similar work,[31] it is claimed that maximum lap shear strength was achieved in comparison with past studies. However, the work will be fruitful to compare when experiments were done with the same process condition as can be seen in Table 3. At constant WS, interface thickness increases then decrease with an increase in TRS. At constant WS of 100 mm/min, with TRS of 800 and 1200 r/min, peelings and flash were observed as the result of inadequate plastic flow and superfluous HI respectively. The Al/Ti interface consists of a layer of solid solution and IMC.

Weld speed. At constant TRS with varying WSs, the interface transformed without considerable deformation and Al–Ti intermixing.[5] The lap joint failure loads decrease with the increase of WS at constant TRS.[76] The defect-free welds were obtained from different process conditions. On the contrary, Wei et al.[75] claimed that the failure load of the joints is dependent upon the WS. It rises with the rise in WS and then decreases for joining Al–Ti lap FSW using a cutting pin. The defect-free welds were obtained at WS 475 mm/min while scrap and voids were observed at WS less than 475 mm/min. A solution of Ti in Al at a mixed layer and Al_3Ti IMC was found at the interface. Similar results were claimed by Chen and Nakata[6] where the critical IMC layer thickness was about 5 μm. Due to diffusion-reaction the Al_3Ti transient phase formed at the interface. It is claimed that an increase in strength is achieved with an increase in WS at constant TRS.[74] Insufficient material flow and too low HI produce macro defects at the top joint surface. However, the placement of work material was different in both cases. At constant TRS, interface thickness decreases then increases with an increase in WS.[31] It is found that at optimum interface thickness better tensile properties were attained. The temperature generated was influenced by the WS and TA. Zhou et al.[79] performed the FSW of AA6061 and Ti6Al4V joints using W-5Re tool with different WSs (40, 80, 120, 160 mm/min) and constant TRS of 1000 r/min. They achieved a maximum failure load of 4026 N at 80 mm/min.

Tilt angle. The TA has a direct influence on the weld penetration. Large TA showed low penetration whereas TA close to zero showed an irregular mixture presenting higher temperatures due to higher torques causing void defects.[77]

Vertical force. The VF showed the WS and the TA to exert greater influence in the joint. The torque is associated with the TRS, WS, and TA. Minimum TRS and maximum WS resulted in maximum torque.[77]

Microstructure. Yu et al.[5] varied TRS at constant WS and found that when TRS 1000 r/min or lower then defect-free joints were obtained, with further increase in TRS leads to surface flash and hook formation as shown in Figure 15. Chen and Nakata[6] found in their study that at constant TRS 1500 r/min with varying

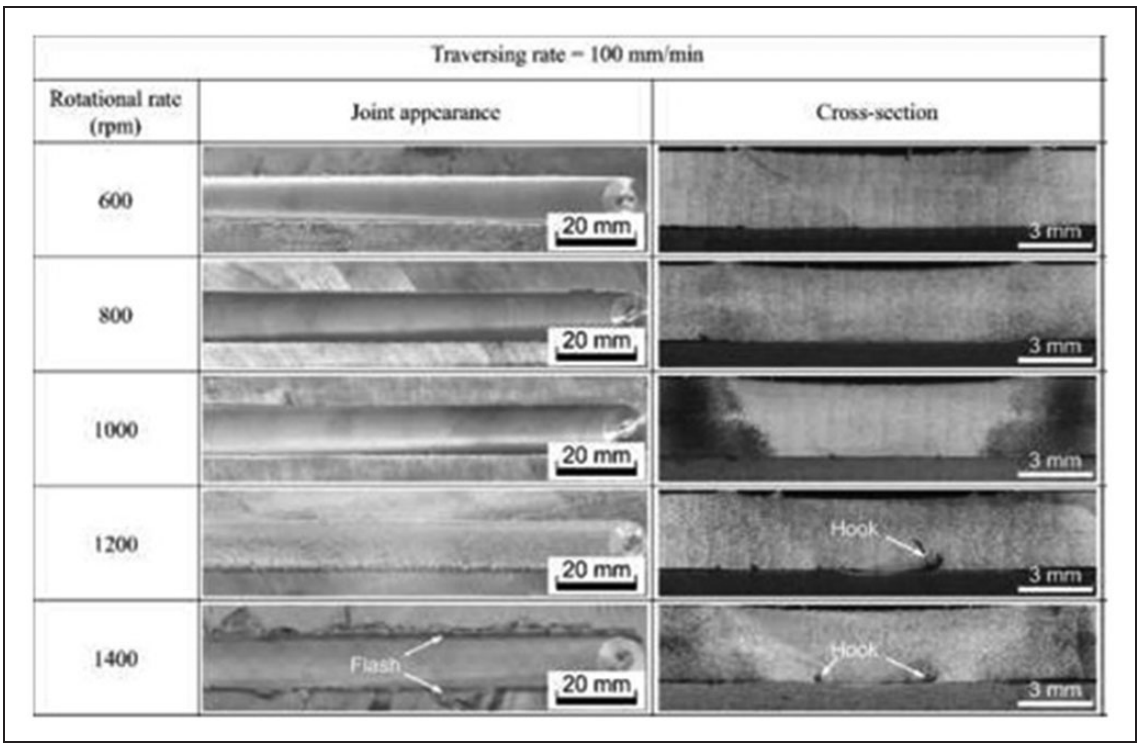

Figure 15. Surface morphology and FSW macrostructure of Al–Ti lap joints at 100 mm/min.[5]

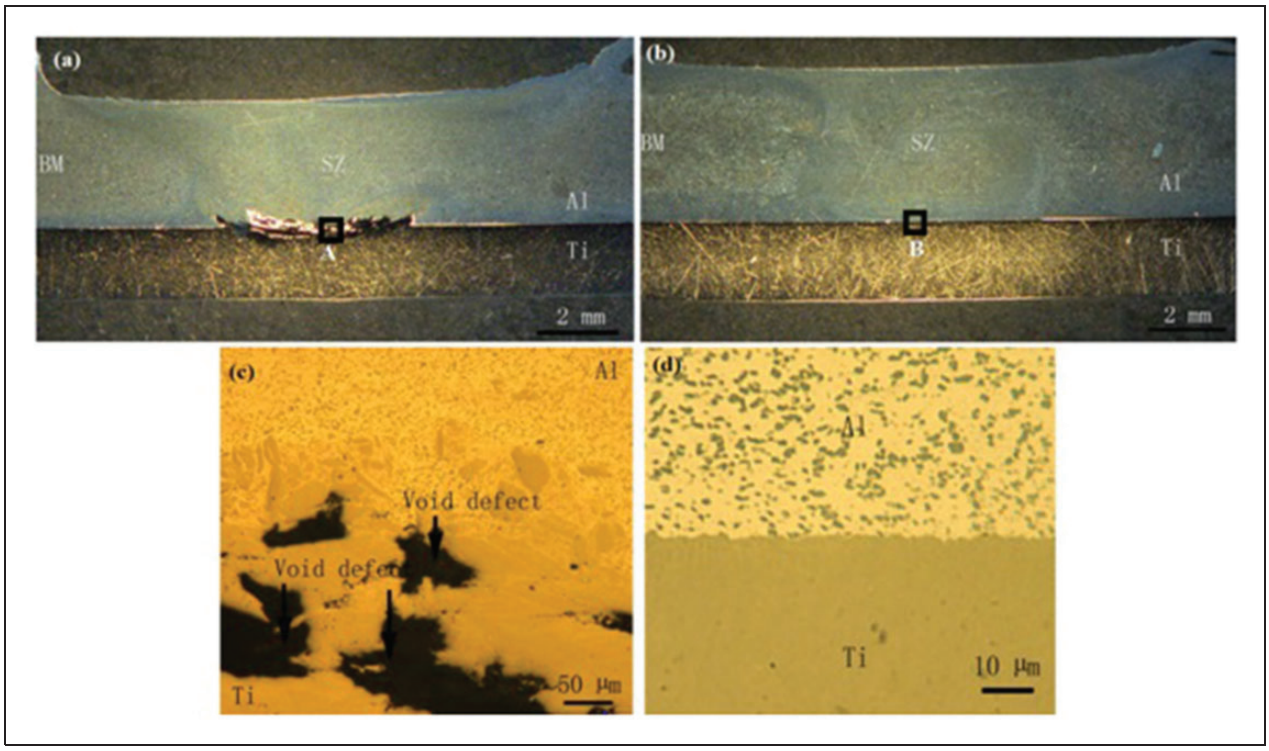

Figure 16. Cross-sections of FSLW Al–Ti joint at TRS 1500 r/min: (a) 60 mm/min, (b) 90 mm/min and interface microstructure (c) region A in (a), (d) region B in (b).[6]
BM: base material; SZ: stir zone.

WS from 60 and 90 mm/min, voids were seen at 60 mm/min due to insufficient Ti metal flow behavior, and defect-free joints with maximum strength were attained at 90 mm/min as shown in Figure 16. The voids observed at WS of 60 mm/min due to probe inserted into lower Ti sheet causing serious softening of upper Al sheet and at higher WS i.e. 90 mm/min, the probe does not touching to surface

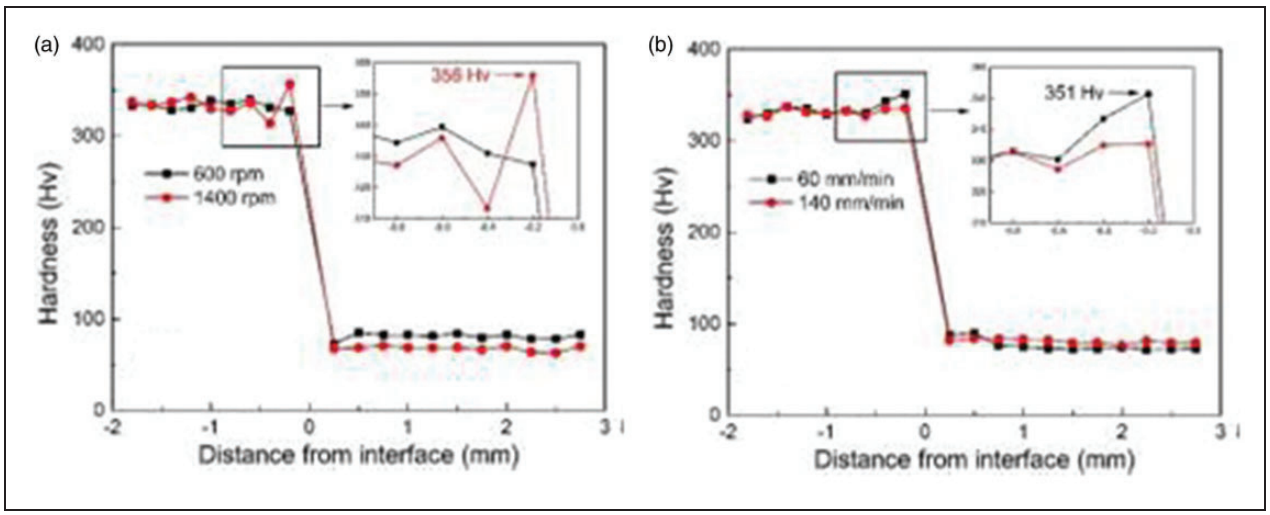

Figure 17. Hardness distribution of the FSW Al–Ti lap joints at (a) WS: 100 mm/min, (b) TRS: 1000 r/min.[5]

of lower Ti sheet which avoids the serious softening of upper Al sheet.

The hardness distribution for Al–Ti (Al BM hardness: 110 HV and Ti BM hardness: 330 HV) FSLWs at different process conditions is shown in Figure 17. There is less variation in hardness on the Ti side ~330 HV, however a sharp decrease in hardness on Al side 78 HV. The large variation in hardness on the Al side is reported due to dynamic recrystallization and the dissolution of precipitates. It is observed that at constant WS (100 mm/min) with increasing the TRS, the average welded Al alloy hardness decrease from 83 HV to 70 HV at 600 and 1400 r/min, respectively. At TRS of 1400 r/min (high HI), the IMCs formed at the joint interface cause an increase in hardness on the Ti side (356 HV). This causes the growth of the grains and precipitates dissipation attributed due to higher HI. Similarly at constant TRS with increasing the WS, the welded Al alloy hardness increase from 75 HV to 80 HV and at 60 mm/min and 140 mm/min, respectively. At WS of 60 mm/min (high HI), the IMCs formed at the joint interface cause an increase in hardness on the Ti side (351 HV). Hence, it is claimed that HI plays an important role in controlling hardness distribution across Al/Ti lap joints.[5,79]

To conclude, for maximum lap shear strength of dissimilar FSLWed joints of Al–Ti alloys, it is recommended that a minimum of ~5 μm the IMC thickness is suitable. FSLW of Al–Ti alloys claimed a maximum shear failure load of ~4.5 kN. To avoid tool erosion, it is recommended to keep lower melting temperature work material on top of higher melting temperature work material. Similar to FSbW, TRS and WS both parameters influence the HI. At low HI, a diffusive interface is produced while at high HI mixed interface is produced with more Ti fragments and a large hook formed. At constant WS of 100 mm/min, with TRS less than 1000 r/min gives. On the contrary, a constant TRS of 1000 r/min, with WS greater than 100 mm/min produces joints without flashes and hooks. Further, the probe length has more influence on the interfacial microstructure and mechanical properties of Al–Ti lap joints. TA has a direct influence on weld penetration. Large TA gives low penetration whereas void defects are produced when TA close to zero. The influence of TA and VF can be explored in terms of microstructure and mechanical properties. It is suggested to optimize the process parameters to get maximum weld efficiency using the design of experiments.

Friction stir spot welding

FSSW or spot FSW or friction spot joining is a derivative of FSW in which WS is absent. Initially, in 2003, this technology was utilized in the Mazda RX-8 rear door panel. It consists of three stages namely tool plunging, dwell, and tool retraction with keyhole (exit hole) as shown in Figure 18. In this section, FSSW and their hybrid processes along with their mechanical and microstructure properties are discussed. Table 4 shows the suggested process parameters and properties of Al–Ti FSSW and other friction-based hybrid processes.

Plaine et al.[36] studied the metallurgical and tensile properties of FSSW of AA6181-T4/Ti6Al4V alloys using TRS of 2500 and 3000 r/min. Defect-free welds were observed and at higher TRS, a lower value of the shear force is attained. A continuous thin reaction layer (Al_3Ti ~0.8 μm thickness) was generated at the Ti–Al interface at the low values of TRS. Further, fatigue strength is moderately larger than the FSSW of Al-related joints. The dissimilar joint efficient performance is attributed due to the reaction layer of the slight quantity of formed IMC with the absence of geometric features. Also,[82] the significance of dwell time (DT) on the tensile properties and interface microstructure of FSSWed joints of

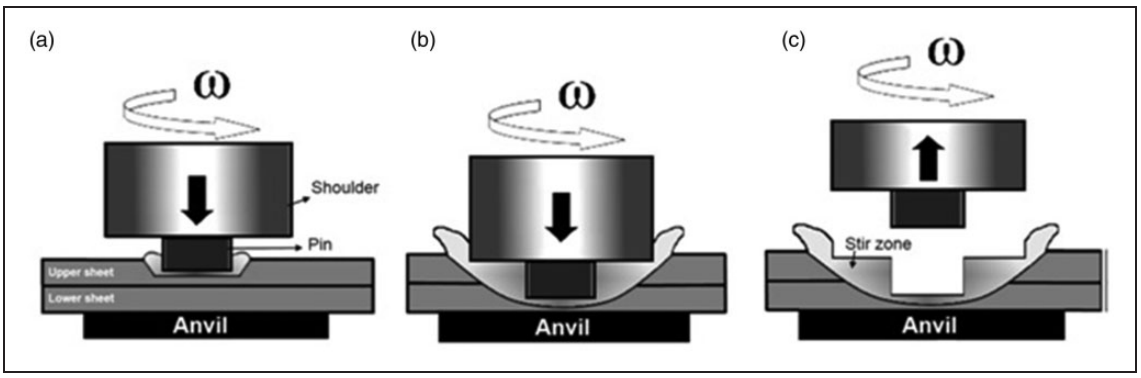

Figure 18. Schematic diagram showing FSSW steps: (a) plunging, (b) dwell, and (c) retraction.[81]

AA5754-Ti6Al4V alloys was evaluated. It is found that DT considerably affects the diffusion process which modifies the interface thickness and hence affects the joint mechanical properties. The result gives an average peak failure load of 7.4 kN with a 2 s DT. The lap shear strength is mainly influenced by the thickness of Al_3Ti IMC, which is considerably changed by DT as depicted in Figure 19. The IMC layer also consists of small precipitates of Al/Fe intermetallics near the Al_3Ti–Ti interface that restricts the growth of Al_3Ti and resulted in fine-grained microstructure.[82] The grain growth of the Al_3Ti is controlled which further resulted in the formation of fine-grains. Plaine et al.[37] studied the effect of TRS and DT on joint strength using response surface methodology (RSM). It was observed that DT has more effect on the joint shear strength (58.9%) where the effect of TRS is not remarkable on the joint performance.

Vacchi et al.[83] investigated the AA6181–Ti6Al4V FSSWed joints for surface corrosion behavior. The corrosion study showed that no much variation in the corrosion potential (E_{corr}) in the various weld zones. However, pitting corrosion resistance in the weld nugget increased than the BM and HAZ due to microstructural changes (Figure 20). The value of potential varies with the type, size, and quantity of precipitates. The precipitates show a cathodic behavior that forms a galvanic cell. A less effective passive film is formed around the precipitate that reduces the potential in HAZ/TMAZ region. Recently in their other work,[90] the effect of the refill FSSW process on the electrochemical corrosion behavior and microstructure of the AA5754-H22 alloy surface of an AA5754-H22/Ti-6Al-4V overlapped joint was analyzed. It is claimed that the process promotes substantial microstructure changes along the joint, which affects the mechanical properties and corrosion behavior of distinct welding regions. The studies indicate that the SZ region has better corrosion resistance than the other refill FSSWed regions (HAZ and BM) due to higher homogeneity and microstructure refinement.

To summarize, for maximum lap shear strength of dissimilar FSSWed joints of Al-Ti alloys, it is recommended that a minimum of ~5 μm the IMC thickness is suitable. The effect of DT on joint strength is more than TRS for dissimilar FSSWed joints of Al–Ti alloys. Similar to FSLW, to avoid tool erosion, it is recommended to keep lower melting temperature work material on top of higher melting temperature work material.

Other friction-based hybrid processes

Many of the researchers have used the concept of hybrid FSW such as UVaFSW, GTAWFSW, FSP, cold gas spraying FSP, friction stir extrusion, etc. as depicted in Table 4. Chen et al.[9] investigated mechanical performance and microstructure of dissimilar joint of Ti6Al4V-2A12 alloys through friction melt-bonded spot welding with Ti over the Al alloy lap joints using a tool without a pin. It is ascertained that superior joints with no keyhole and hook defects were found than FSSW and resistance spot welding. Moreover, the mechanism of bonding depends on the diffusion and Ti and Al reaction, which forms a nanoscale Al_3Ti IMC. Khodabakhshi et al.[87] evaluated the bond interface structure between Ti fragments placed on an Al alloy substrate by the spray of cold gas after FSP. It can be seen that the adiabatic shear interlocking bonding mechanism is supported by a chemical bonding through deformation which results in Al_3Ti intermetallic reaction layer formation with ~10–20 nm thickness. Huang et al.[10] developed a friction surfacing-assisted hybrid FSW (FS-HFSW) method to enhance the efficiency of the joint and prevent the pin wear for welding of Ti6Al4V and AA2A12 alloy. It is revealed that the defect-free welds with the highest joint efficiency of 85.3% of the base Al alloy. Due to the combined effects of complex mechanical interlocking and $TiAl_3$ IMCs layer, the excellent joint was achieved (Figure 21).

The use of ultrasonic vibration has played a crucial role in diverse areas due to the key benefits to material processing as it reduces energy consumption and

Table 4. Summary of suggested parameters and findings of Al–Ti FSSW and friction-based hybrid processes.

WP materials	Process	AS–RS	Thk	Tool design	Parameters	Findings	Ref
AA6181-T4–Ti6Al4V	FSSW	Al on top of Ti	Al: 1.5 mm Ti: 1.5 mm	PD: 1.4 mm, DT: 3 s, CF: 12 kN	TRS: 2500 and 3000 r/min	Ultimate lap shear force 6449 $\pm$ 554 N at TRS: 2500 r/min, 0.8 μm thickness interface layer formed	36
AA5754–Ti6Al4V	FSSW	Al on top of Ti	Al: 2.0 mm Ti: 2.5 mm	TM: Mo–V alloyed hot work tool steel tool, diameters of clamping ring diameter: 14.5 mm, sleeve diameter: 9 mm, PD: 6 mm	TRS: 1800, 2000, 2200 r/min; DT: 2, 5, 8 s	DT has more influence on lap SS than TRS and DT interaction. Optimum parameter: TRS: 2000 r/min, DT: 2 s	37
AA5754–Ti6Al4V	FSSW	Al on top of Ti	Al: 2 mm Ti: 2.5 mm	PD: 1.8 mm, DT: 0–5 s, CF: 12 kN, clamping ring diameter: 14.5 mm, threaded sleeve diameter: 9 mm, threaded pin diameter: 6 mm, plunging and retracting rate of sleeve:1.8 mm/s	TRS: 2000 r/min	Maximum SS: 7.4 kN with DT: 2 s, critical IMC thickness: 5 μm which is directly influenced on the tensile strength and the bending ductility	82
AA6181-T4–Ti6Al4V	FSSW	Al on top of Ti	Al: 1.5 mm Ti: 1.5 mm	clamping ring diameter: 18 mm, sleeve diameter: 9 mm, pin diameter: 6.4 mm, PD: 1.4 mm, DT: 3 s, CF: 12 kN	TRS: 2500 r/min	H: 95 $HV_{0.3}$, pitting corrosion resistance is increased in the weld	83
AA6061–Ti6Al4V	FSSW	Al on top of Ti	Al: 4 mm Ti: 4 mm	TM: WC–Co-based alloy, SD: 17mm, RD: 5 mm, PL: 5.8 mm	TRS: 1000, 1400 r/min, DT: 10, 15 s	Maximum shear load: 4.2 kN with low hardness at TRS: 1000 r/min, DT: 10 s	84
2A12-T4–Ti6Al4V	FMSW	Ti on top of Al	Al: 4 mm Ti: 1.5 mm	TM: GH4169 superalloy, SD: 16 mm and without pin, PD: 0.6 mm, DT: 100 s	TRS: 1180 r/min	Maximum tensile shear load: 18.2 kN than FSW (7.4 kN) and RSW (6.16 kN) with no keyhole and no hook defects formed	9
AA5083–pure Ti powder	FSP & water-FSP	-	Al: 5 mm, Ti: Avg. particle size: 23 μm	TM: WC–13 wt% Co, SD: 15 mm, PSP: SC, RD: 6 mm, PL: 4.5 mm, PD: 0.2 mm	TRS: 1400 r/min, WS: 40 mm/min, TA: 2°	FSP peak temp. in the air: 442°C with, FSP Peak temp. in water: Diffusion layer thk. in the air-FSPed AMCs:	85

(continued)

Table 4. Continued.

WP materials	Process	AS–RS	Thk	Tool design	Parameters	Findings	Ref
						~4 μm, whereas in water-FSPed AMCs: ~2.7 μm. Avg. grain size in air FSPed AMCs: 3 μm, whereas in water-FSPed AMCs: 1 μm, UTS of air and water-FSPed AMCs: 383 ± 4 MPa &423 ± 7 MPa	
AA 5052 as-cast TiO_2 powder	FSP	Al-Al, butt	Al: 6 mm, TiO_2 powder:2 μm	PL: 4.5 mm	TRS:700, 1000, 1300 r/min, WS: 50, 65 and 80 mm/min	Defect-free FSP produced with a decrease in the groove width. H: 78 ± 1 Hv, TS: 193.1 ± 3 MPa at TRS: 1000 r/min, WS: 65 mm/min	86
AA5083-H34–pure Ti powder	cold gas spray coating followed by FSP	-	Al: 10 mm Ti: particle size: 20–80 μm	A Ti coating layer thk. ~ 800 μm deposited on the Al substrate. TM: WC pin less tool, SD: 12 mm, PD: 0.5 mm	TRS: 900 r/min, WS: 63 mm/min, TA: 2.5°	Avg. intermetallic reaction layer thickness: ~10 nm within an inter-diffusion distance of ~600 nm	87
TC4 (bottom substrate)–6082-T6 (middle coating layer)–2A12 Al (top lap)	FS-HFSW (FS followed by FSLW)	Al on top of Ti	Al 2A12: 3 mm Al 6082-T6: 20 mm dia.	PSP: TCH together with the enlarged head (with a diameter of 8 mm), SSP: Concave	TRS: 1800 r/min, WS: 90 mm/min, VF: 3 kN	Avg. measured deposition layer thickness: 0.23mm. Max. tensile load: 12.2 kN (85.3% of Al) at TRS /WS =20	10
AA6061–Ti6Al4V	UVaFSLW	Al on top of Ti at RS	Al: 3 mm Ti: 2 mm	TM: WRe5 and WRe25, PL: 2.9 mm, PD: 0.1 mm, SD: 12 mm, PSP: TC, RD: 4 mm, TD: 3 mm, ultrasonic frequency: 20 kHz, Amplitude: up to 20 μm, Pressure: 0.1–0.5 MPa, distance between the ultrasonic horn and the FSW tool: 25 mm	TRS: 1000 r/min, WS: 100 mm/min	Reduce TW with PL: 2.9 mm (WRe5), maximum load: 415.0 N/mm (~ 225 % of FSLW of Al-Ti) with a 10 μm amplitude, and pressure: 0.3 MPa	38
AA 6061-T6–Ti6Al4V (TC4)	UaFSW	Ti-Al	Al: 2 mm Ti: 2 mm	TM: W-Re, SSP: Concave, SD: 12 mm, PSP: TCH, PL: 1.9 mm, RD: 6 mm,	TRS: 650 r/min, WS: 180 mm/min, TA: 2.5°	Avg. SZ grain size of FSW: ~7.8 μm and in UaFSW: 5.7 μm	11

(continued)

Table 4. Continued.

WP materials	Process	AS–RS	Thk	Tool design	Parameters	Findings	Ref
				TD: 4 mm, SPR: 2, PD: 0.05 mm, the distance between ultrasonic generator and butt joint line: 20 mm		TS: 236 MPa (85% of Al), EL: 3.3% (UaFSW) while TS: 182 MPa, EL: 2.1%, lowest micro-hardness: 68% of Al.	
AA 6061-T6–Ti6Al4V	GTAWaFSW and GTAW	Ti–Al	Al: 3.5 mm Ti: 3.5 mm	TM: WC–12% Co, SD: 18 mm, RD: 5 mm, PL: 3.3 mm, the distance between GTAW torch and FSW tool: 20 mm	TRS: 300,400,450 r/min, WS: 60,72,84 mm/min, VF: 22.5–35.3 kgf, TA: 3°, TPO: 2 mm to Ti side	In HFSW: max. TS: 300MPa (91% of Al), EL: 2.8% at 350 r/min In FSW: max. TS: 230MPa (70% of Al), EL: 1.2% at 400 r/min.	88
2024-T4–Grade 2 Ti	Friction stir extrusion	Al on top of Ti	Al:6.35 mm Ti: 6.35 mm	TM: O1 hardened tool steel, concave groove 15 mm from the edge of Ti, o-ring groove of 3 mm depth, 48° included angle and neck diameter of 3 mm, SD: 25.4 mm, SSP: 7° convex with six scrolls, PSP: threaded, RD: 6.35 mm, PL:4.6 mm, PD: 5.3 mm into Al	TRS: 500, 700, 900 r/min, WS: 38, 50.8, 76.2, 101.6 mm/min, TA: 0, 1.5°, TPO: 2 mm from center of groove to the advancing side	Good joints obtained at TRS: 700 r/min, WS: 38.1 mm/min. Shear strength up to 70% of the parent material. Groove geometry is an important parameter. No intermixing hence minimization of IMCs	89

TM: tool material; SSP: shoulder surface profile; SD: shoulder diameter (mm); PSP: probe surface profile; TC: taper cylindrical or conical; SC: cylindrical; PD: plunge depth (mm); PL: probe length (mm); RD: root diameter (mm); TD: tip diameter (mm); SPR: shoulder-to-probe diameter ratio; TRS: tool rotational speed (r/min); WS: weld speed (mm/min); TA: tool tilt angle (°); VF: vertical force; TPO: tool probe offset; thk: thickness (mm); EL: elongation (%); H: hardness; DT: dwell time (s); CF: clamping force (kN); SS: shear strength; FMSW: friction melt-bonded spot welding; RSW: resistance spot welding; FS-HFSW: friction surfacing followed by friction stir lap welding; UVaFSLW: ultrasonic vibration-assisted friction stir lap welding- TW: tool wear- UaFSW: ultrasonic-assisted friction stir welding; TCH: threaded conical; IMC: intermetallic compounds; GTAWaFSW: gas tungsten arc welding-assisted friction stir welding.

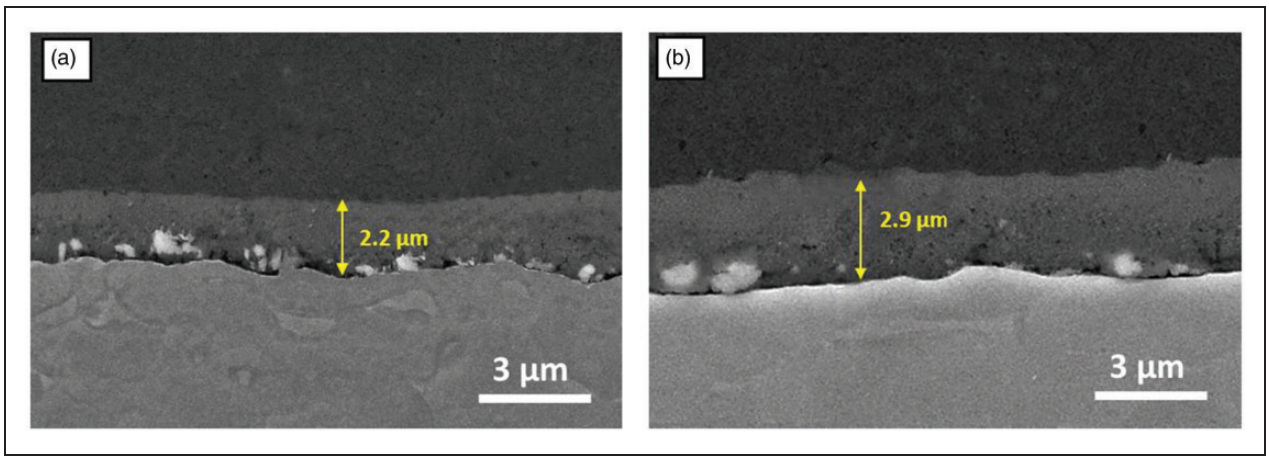

Figure 19. Backscattered micrograph of the Ti6Al4V and AA5754 alloys FSSWs at dwell time of (a) 8 s and (b) 10 s.[82]

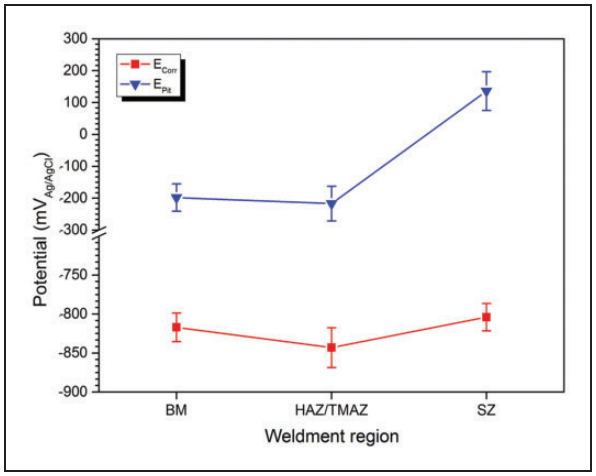

Figure 20. Corrosion (Ecorr) and pitting (Epit) potential in 0.01 M NaCl and 0.1 M Na_2SO_4 solution of various regions of FSSWed AA6181.[83]
HAZ: heat-affected zone; TMAZ: thermomechanically affected zone.

process cost. Many of the manufacturing techniques have employed assisted ultrasonic vibrations for improving the properties of the final products.[91] Yu et al.[38] fabricated joints of AA6061 and Ti6Al4V alloys using ultrasonic-assisted FSW (UaFSW). Their results are promising which showed the elimination of tool wear. With this approach, plastic flow and dynamic recrystallization were enhanced compared with conventional FSLW. The lap shear strength was found to be doubled because of the ultrasonic vibration effect. Figure 22 indicates the comparison of pin length variation of W-based tool pin with FSLW and UaFSLW. Ma et al.[11] studied UaFSW of Al6061-T6 and Ti6Al4V alloys. They employed low HI with the small depth of plunge and TPO due to which the diffusion bonded layer without IMCs was produced and the improvement in the diffusion layer was noticed. At the bottom interface, a hook-like structure was formed which has a good amount of mechanical interlocking and bonding length. The maximum tensile strength attained 236 MPa (85%) of the parent Al alloy and 54 MPa higher than the conventional joint. The microhardness of the SZ was enhanced because of the refinement of grain, which is induced by ultrasonic. No IMCs layer, pore, or microcrack was observed at the weld interface which is well supported by Yu et al.[38] and Zhou et al.[43]

Patel et al.[60] joined AA6061–pure Ti using the cooling and heating conditions of FSW. The following cooling media such as CO_2, compressed air, and water at a measured flow rate under cooling conditions was employed. While heating-assisted FSW (HFSW) was carried out with a heat source at different current densities just before the FSW tool. FSW with water cooling assistance condition exhibited superior joint properties. On the contrary, weld joint strength was found worst due to decreased cooling rate in compressed air, CO_2 cooling assisted FSW as well as in HFSW. Several microcracks at the interface were seen in NFSW and water FSW samples. Similarly, multiple voids in the SZ were observed in $CFSW_{air}$ and $HFSW_{40A}$. It is claimed that Al–Ti, Ti_4Al, and Ti_3Al_2 IMCs in the various processing conditions of NFSW, $CFSW_{WATER}$, and $HFSW_{60A}$, respectively.

Bang et al.[88] studied the effect of GTAW to preheat the Ti alloy in FSW of Al6061-T6 and Ti6Al4V alloys on mechanical and microstructural properties. It is found that the strength was 91% for Al alloy parent metal and 24% more than FSW welds without GTAW at the same weld condition. The elongation was observed twice than conventional FSW welds with improvement in the strength of the joint. Huang and Shen[85] investigated microstructure, mechanical properties, and interfacial bonding of the interface of FSPed of Ti-AA5083 composites with AA5083 sheet and Ti particles both in water and air environment. The finer equiaxed grains (average size$\sim$1 µm) and a maximum amount of LAGBs in

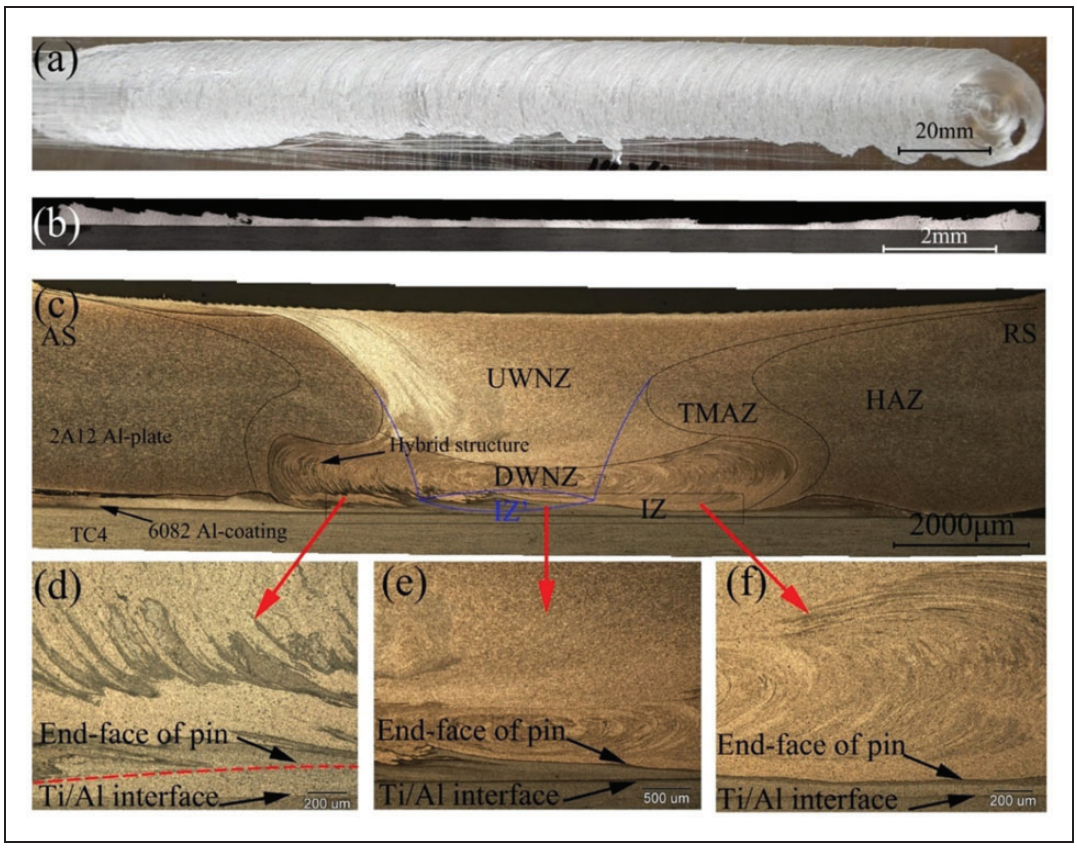

Figure 21. (a) Morphology of Al-coating and (b) cross-section; (c) macrostructure of FS-HFSW joint, (d–f) distance between the Ti–Al interface and the pin.[10]
HAZ: heat-affected zone; TMAZ: thermomechanically affected zone; UWNZ: up weld nugget zone; DW: down weld nugget zone.

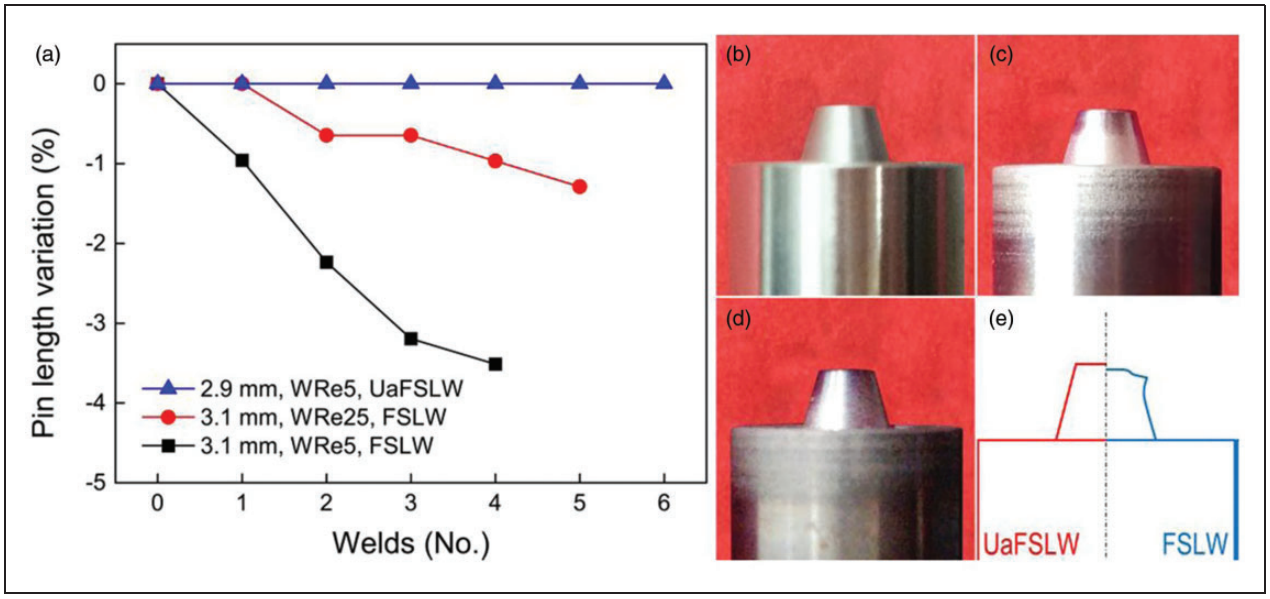

Figure 22. Wear of tool in FSLW and UaFSLW: (a) pin length variation, (b) original tool geometry, (c) tool after three UaFSLW welds, (d) tool after six UaFSLW welds, (e) tool comparison between UaFSLW and FSLW.[38]
FSLW: friction stir lap welding; UaFSLW: ultrasonic-assisted friction stir welding.

water-FSPed AMCs. Further, using both methods, a quite uniform Ti particle distribution with superior interface bonding of Al–Ti was achieved with no micropores, and detrimental reaction products were obtained. It was suggested that Ti_3Al, TiAl, $TiAl_2$, Ti_2Al_5, and Al_3Ti IMCs formed at the interface. The tensile test results showed that water-FSPed AMCs have higher YS (265 MPa) and UTS

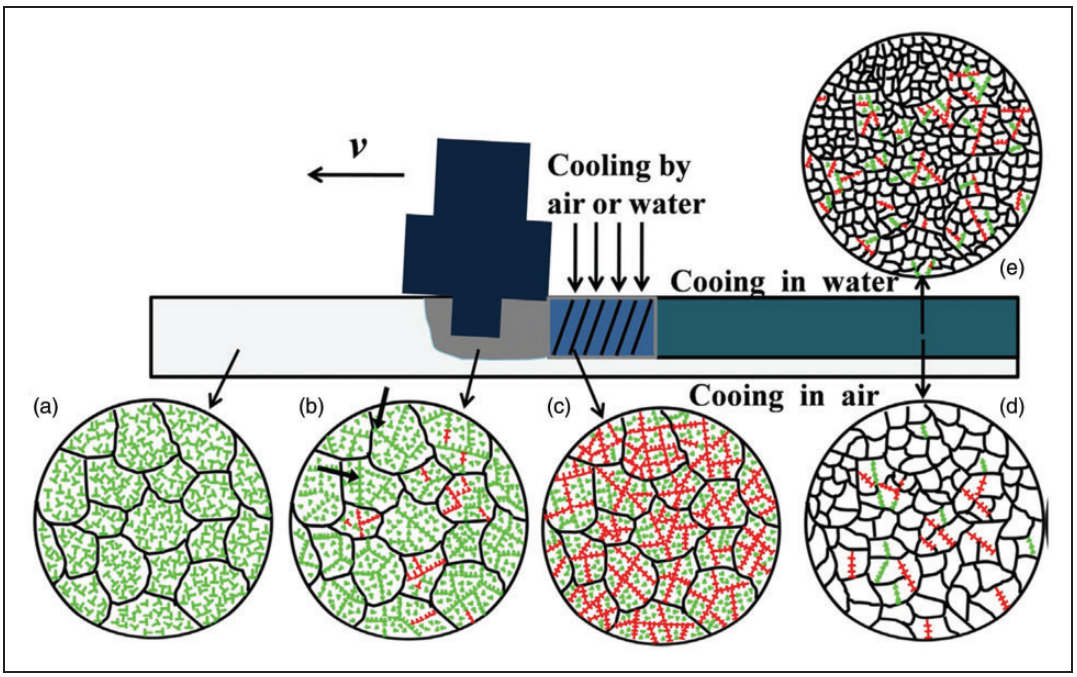

Figure 23. Schematic diagram showing microstructural changes that take place at different stages of fabricating AMCs by FSP: (a) the original microstructure; (b) the microstructure during FSP; (c) the microstructure when FSP tool just left; (d) and (e) the microstructure at air and water cooling, respectively.[85]

(423 MPa) in comparison with the AA5083 matrix with the ductility of about 15% and the air-FSPed AMCs. The faster cooling rate in water-FSPed AMCs produces smaller particles with a high amount of subgrain boundaries and LAGBs in comparison with air-FSPed AMCs as can be seen in Figure 23.

Evans et al.[89] successfully created AA 2024-T4 to cp Ti lap joints using the friction stir extrusion (FSE) process. In their earlier work, they applied the same process to join Al–steel.[92] It is a modification of the lap FSW process wherein the material is extruded into a preformed concave groove. It is claimed that the process creates a better dissimilar material joint by eliminating the issues of IMCs. It is[89] showed that successful joints were produced at TRS: 700 r/min and WS: 38.1 mm/min with up to 70% shear strength of parent material. Further, the groove geometry is a vital parameter for joint strength.

To conclude, the friction-based hybrid approaches like UVaFSW, GTAWFSW, FSP, cold gas spraying FSP, FS-HFSW, underwater or cooling-assisted FSW claimed a comparable increase in the joint efficiency in contrast to normal FSW. Such processes can be explored and an in-depth understanding of their underlying physics along with each of the process parameters.

Diffusion bonding and other processes

Diffusion bonding. It is a solid-state joining technique where the joint is achieved with the application of heat and pressure at the finite interval, well below the melting temperature of metals without employing secondary phases, solvent, or liquid. A schematic diagram showing the die setup for the diffusion bonding (DB) process is shown in Figure 24. Due to slower heating and cooling rates, the atoms can fully diffuse in the weld joint. Table 5 shows the recommended parameters and properties of Al–Ti DB and other processes.

Wei et al.[93] studied pure Ti–Al alloy diffusion bond joint process formation. It is claimed that the joint process formation took place in the following way as first Ti and Al elements interdiffuse to form a solid solution, latter only Al_3Ti phase is produced using diffusion-reaction under a particular range of holding time, forming a layer, which grows according to the parabolic law. The joint strength reaches or exceeds the strength of pure Al due to the Al_3Ti layer. At a constant hold time of 60 min with an increase of bond temperature, the microstructure of Ti side fracture surfaces gets highly diffused. On the contrary, at a constant bond temperature of 650°C with a different hold time, initially after 10 min grain phases were formed and gradually grow. A time delay before the diffusion-reaction was revealed which is ~60 min hold time with a bond temperature of 625°C but less than 10 min hold time with a bond temperature of 650°C. Hence, the effect of the bond temperature at constant hold time is much clearer than the effect of the hold time at each bond temperature. Three IMC phases Ti_3Al, TiAl, and Al_3Ti exist.

Rajakumar and Balasubramanian[32] developed empirical expressions for predicting the joint shear

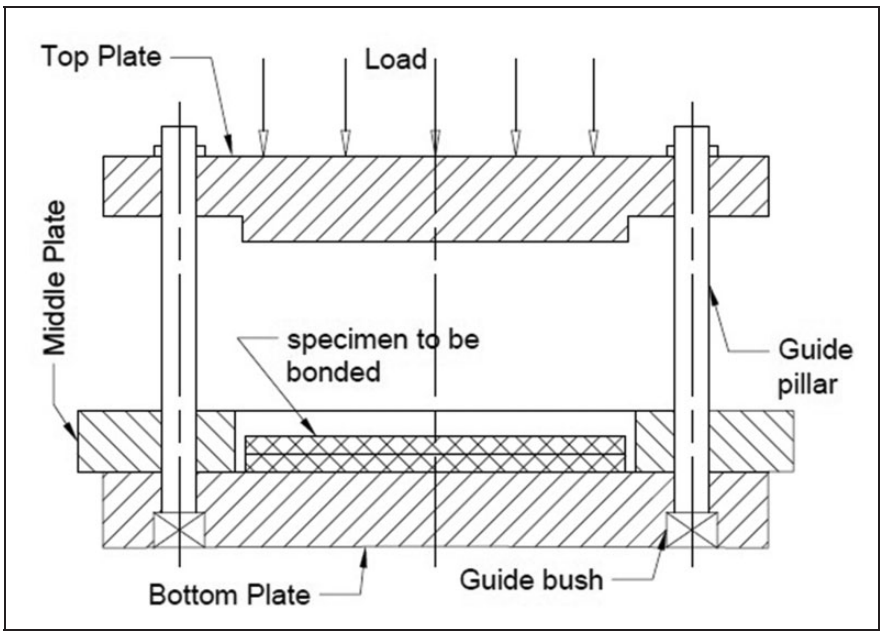

Figure 24. Schematic diagram showing die setup of the diffusion bonding process.[32]

strength, the interfacial layer thickness, and the hardness of weld interface diffusion-bonded cp Ti–AA7075 Al alloy using RSM. It has been observed that bonding temperature plays a vital role in bonding characteristics followed by bond pressure and hold time. The joint shear strength and interface layer thickness are the functions of bonding temperature and IMCs grow steadily in a gradual manner with an increase in bond temperature. The interface layer thickness increases with bonding temperature and holding time. The bonding pressure has less effect than bonding temperature and holding time. A maximum of 87 MPa shear strength, a maximum of 163 HV hardness, and optimum thickness of interface layer 7 μm, at 15 MPa bond pressure, at 510°C bond temperature and 37 min hold time was reported.

Jiangwei et al.[33] successfully joined Ti and Al using a DB process. They found two zones at the Ti–Al interface zone namely transition region on Ti substrate, Al coating, and transition region on Al substrate. At the transition region on the Ti substrate and aluminized coating, TiAl and Al_3Ti were formed, but intermetallic was absent in the transition region on the Al substrate. Further by controlling the process parameters the intermetallics width at the joint interface can be reduced. It is seen from Figure 25 that the transition region microhardness on the Al substrate is maximum (point 6), the microhardness in the transition region on the Ti substrate (point 5), and that of Al coating (point 7) were superior to Ti and Al substrate. Alhazaa and Khan[94] successfully diffusion bonded Al7075 to Ti6Al4V alloys with tin-based alloy as insert material and Cu coating. It is observed that a strong joint is produced at the joint interface due to the diffusion of Ag and Cu into the Al alloy. Microhardness and shear strength are directly related to bond time. An increase in the bond time increases the microhardness and shear strength at the joint region due to the presence of intermetallics. According to the "solder bonding" process, the IMC formation at the bonding interface takes place due to the diffusion of Sn in Ti6Al4V. Also, several intermetallics such as "Al_2Cu, $CuSn_3Ti_5$, $MgZn_2$, Ti_3Sn, Al_3Ti, Sn_3Ti_5, Mg_2Sn, and $AgMg_3$"[94] were produced.

Transient liquid phase bonding. TLP bonding or diffusion brazing is a class of solid-state DB technique wherein an interlayer is positioned among the abutting surfaces, is heat up over its melting point, and diffuses in the parent metal. A schematic diagram of TLP bonding is depicted in Figure 26. Similar to other welding processes, defects like segregation, deformation, crack, etc. slightly occur.[33] Alhazaa et al.[96] investigated the TLP bonding of Ti6Al4V and Al7075 alloys employing Cu interlayer for different bond times. Three different phase structures were seen namely, "θ (Al_2Cu), T($Al_2Mg_3Zn_3$), and $Al_{13}Fe$"[96] in the Al alloy. On the contrary, Cu_3Ti_2 intermetallic was observed in the Ti alloy. A metallurgical joint was formed by a process of isothermal solidification when bonding time (BT) increase to 30 min. The value of microhardness shows a marginal variation across the bond interface with the absence of the IMC formation at the bonding interface. Kenevisi and Khoie[39] joined Al7075 to Ti6Al4V alloy with Sn-based alloy as insert material via the TLP bonding process. A relatively good bond is achieved with coated Cu surfaces of Al alloy and Ti alloy with Sn-based alloy as insert material. The joint strength is a

Table 5. Summary of suggested parameters and findings of Al–Ti diffusion bonding and other processes.

WP materials	Process	Joint	Thk	Interlayer	Parameters	Findings	Ref
cp Ti/AA 7075	Diffusion bonding	Al on top of Ti, Lap	Al: 5 mm Ti: 5 mm	–	BT: 425, 475, 525°C; BP: 5, 13, 20 MPa; HT: 5, 25, 45 min	Maximum SS: 87 MPa, H:163 HV, and IMC thickness: 7 μm at BT: 510°C, BP: 17 MPa, and HT: 37 min	32
TA2-Al L4	Diffusion bonding	Lap	Al: 3 mm Ti: 3 mm	–	BT: 640°C; BP: 24 MPa; HT: 90 min; and the max vacuum degree: 1.12–2.66 $\times$ 10^{-3} Pa	Transition zone micro-hardness: 420–570 HM	33
cp Ti TA2-Al L4	Diffusion bonding	Lap	Al: 10 mm Ti: 5 mm	–	BT: 500, 550, 600, 625, 650°C; HT: 10–600 min; static pressure: 5 MPa; heating rate: 60°C/min; vacuum degree: 2.5–3.0 $\times$ 10^{-3} Pa	Joint strength depends on the percentage of met-allurgical combination and structure of inter-face in the diffusion zone, and it can reach or exceeds the strength of pure Al after Al_3Ti	93
Al7075–Ti6Al4V	Diffusion bonding	Lap	Al: 3 mm Ti: 3 mm	Sn–3.6Ag–1Cu	BT: 500°C; BP: 1 MPa; HT: 10–60 min; electrode-position of Cu onto Al7075–Ti6Al4V; DB using interlayer; Vacuum: 3 $\times$ 10^{-4} Torr	Joint SS increases with BT and HT. Maximum H: 141 VHN at HT: 60 min	94
AMg6-OT4	Diffusion bonding	Butt	16mm diameter	Ti–Al composite	BP: 2–10 MPa; HT: 15–90 min; Vacuum: 2.66 Pa	Joining these materials through Ti-Al compos-ite interlayer is an example of the DB for dissimilar materials	95
2024–Ti6Al4V	TLP	Lap	Al: 5 mm Ti: 5 mm	Cu – 22%Zn	BT: 510°C; BP: 1 MPa; Vacuum: 0.01 Pa; 50 μm thick Cu – 22%Zn interlayer	Highest SS: 37 MPa, H: 153 VHN at HT: 60 min	12
2024–Ti6Al4V	TLP	Ti-Ti & Al-Ti	-	Sn–5.3Ag–4.2Bi	50 mm thick Sn–5.3Ag–4.2Bi interlayer; Ti–Ti for 620°C for 60 min; Al–Ti for 453°C for 180 min.	TS: 62 MPa for Al–Ti joint as compared with 7.8MPa for the control sample	14
Al7075–Ti6Al4V	TLP	Lap	Al: 3 mm Ti: 3 mm	Sn–4Ag–3.5Bi	BT: 500°C Vacuum: 5 $\times$ 10^{-4} Torr; Electrodeposition of Cu onto Al7075–Ti6Al4V;	Highest SS: 36 MPa at BT: 60 min. H increases with HT	39

(continued)

Table 5. Continued.

WP materials	Process	Joint	Thk	Interlayer	Parameters	Findings	Ref
					50 μm thick Sn–4Ag–3.5Bi interlayer		
Al7075–Ti6Al4V	TLP	Lap	Al: 3 mm Ti: 3 mm	Cu	BT: 500°C; BP: 0.2 MPa; Vacuum: 3×10^{-4} Torr; 22 μm thick Cu interlayer	Highest SS: 19.5 MPa, H: 170 VHN, at HT: 30 min	96
6082–Ti Grade 2	TLP	Al-Ti	ø 20 × 15 mm	Ag72Cu28 grade silver 0.05 mm thick strip	HT: 15, 30, 60 min; Vacuum: 10^{-4} to 10^{-5} mbar; specimen heating rate: 30–40°C/min; brazing temperature: 520–580°C	shear strength of 20 MPa at brazing temperature: 530°C, HT: 30 min	97
6061–Ti6Al4V	Brazing	Ti on top of Al, Lap	Al: 3 mm Ti: 1 mm	Al–8.4Si–20Cu–10Ge and Al–8.4Si–20Cu–10Ge–0.1Re: 200 μm thick	Vacuum furnace under Ar atmosphere at 530°C	Joint strength is improved by adding rare earth elements	98
Ti Grade 2 – $TiAl_{48}Cr_2Nb_2$	diffusive brazing	butt	-	B-Ag72Cu-780, CF032A, Ni99.0: 0.05 mm thick	Vacuum: 10^{-3} to 10^{-5} mbar	Highest SS: 264–303 MPa for Ti grade 2 brazed joints at 1030°C brazing temperature, HT: 30 min using B-$Ag_{72}Cu_{780}$ interlayer and 1030°C brazing temperature, HT: 1 min using Cu interlayer	99
AA6061–Ti6Al4V	Ultrasonic welding	Al on top of Ti, Lap	Al: 1 mm Ti: 0.4 mm	pure Al interlayer	BP: 0.552 MPa; 4.0 kW and frequency: 20.0 kHz, Vibration amplitude: 70 μm; Energy input: 500–1100 J in 150 J steps	SS: 106 MPa at Energy input: 1100 J. Failure mode changed from interfacial to pull-out, when energy input exceeds 950 J	15
AA6061–Ti6Al4V	Ultrasonic welding	Al on top of Ti, Lap	Al: 0.3 mm Ti: 0.3 mm	–	HT: 90, 110, 140, 170, 200 ms; BP: 0.3, 0.4, 0.5 MPa; 3.2 kW; Frequency: 20 kHz	Width of the diffusion layer increases with increase in HT. strongest joint obtained at optimal process parameters BP: 0.4 MPa and HT: 170 ms	27
AA6061–cp Ti	ultrasonic spot welding	Al on top of Ti	Al: 1.5 mm Ti: 1 mm	Clamping pressure: 15 MPa and vibration: 32 μm	Weld time: 0.6–1.4 s	Neither IMC nor significant interfacial reaction layer formed even	43

(continued)

Table 5. Continued.

WP materials	Process	Joint	Thk	Interlayer	Parameters	Findings	Ref
						under 1.4 s. Max. shear load: 5128 N at weld time:1 s.	
AA2139-T8–Ti6Al4V	ultrasonic spot welding	Al on top of Ti, Lap	Al: 1 mm Ti: 1 mm	–	BP: 0.55 MPa; HT: 0–4 s; 2.5 kW; Frequency: 20.5 kHz; Welding energy: 4 kJ	Peak failure load: 5.3 kN (∼100 MPa, SS). IMC layer was absent.	100
Al4N–cp Ti AA7075-T6–Ti6Al4V	ultrasonic torsion welding	Al on top of Ti, Lap	Al: 2 mm Ti: 1.5 mm	–	6.5 kW and continuous sine wave at frequency: 20 kHz; welding energy: 450–2200 J, Amplitude: 18–50 μm, Welding force: 800–2000 N	Optimized process parameters for Al4N-cp Ti joints – Welding energy: 500 J, Amplitude: 24 μm, Weld force: 1300 N, HT: 0.53s, Avg. tensile SS: 15.2 $\pm$ 0.5 MPa; Optimized process parameters for AA7075-T6–Ti6Al4V joints – Welding energy: 1900 J, Amplitude: 46 μm, Weld force: 2000 N, HT: 1.1s, Avg. tensile SS: 41.4 $\pm$ 3.7 MPa	101
AA1199–cp Ti	ultrasonic torsion welding	Al on top of Ti (vis-a-verse), Lap	Al: 0.8 mm Ti: 0.8 mm	–	Maximum generator power of 6500 W; Maximum force: 3000 N	For Al/Ti joint: TS: 15.2 $\pm$ 0.5 MPa at WE: 500 J, OA: 24,WF: 1300, WT: 0.53 s, UJT: 234°C, LJT: 231°C For Ti/Al/ joint: TS: 6.5 $\pm$ 0.4 MPa at WE: 1800 J, OA: 47, WF: 1100, WT: 0.95 s	102
Al: 99.2; Mg: 0.2 and Ti: 90.0; Al: 6.1; V: 3.9	EMW	Axial joint	Al: 20 mm OD and WT: 2 mm	–	12 kJ generator; Voltage: 7.9 kV; Gap: 2 mm	Mechanical interlocking and IMCs are the main factors for EMW	103
Al99.5 and TiAl6V4	EMW	Ti on top of Al, Lap	Al: 20 mm OD and WT: 1 mm, Ti: 15 mm OD and WT: 2.5 mm	–	IV: 10 m/s up to 130 m/s; impact angle (α): 5°; Gap: 1.5 mm	Optimum joint IV: 100 m/s	104

IMC: intermetallic compounds; DB: diffusion bonding; BT: bonding temperature; BP: bonding pressure; HT: holding time; H: hardness; SS: shear strength; TLP: transient liquid phase bonding; EMW: electromagnetic or magnetic pulse welding; OD: outer diameter; ID: inner diameter; WT: wall thickness; IV: impact velocity; WE: welding energy; OA: oscillation amplitude; WF: welding force; WT: welding time; UJT: upper joint temperature; LJT: lower joint temperature; thk: thickness (mm); TS: tensile strength.

function of BT and attained at 36 MPa at 60 min. It is seen from Figure 27 that at smaller BT lower value of hardness was obtained than other BTs, which is attributed to the presence of soft interlayer. Increasing BT reduces the joint region width. It was found that the following intermetallic phases "Al_2Cu, Mg_2Sn, Cu_3Ti_2, $AgMg_3$, TiAl, Ti_3Al, Ag_2Al, Cu_3Ti, and Sn_3Ti_5"[39] were produced at the bonding interface through the TLP bonding.

Samavatian et al.[12] studied the TLP bonding of Al 2024 and Ti6Al4V alloys using 50 μm thick Cu – 22% Zn interlayers for various BTs. It is observed that because of the existence of interlayer, Al_3Ti IMCs at the bonding interface are reduced. The high value of shear strength of 37 MPa reaches in an hour due to various IMCs formed. It is claimed that "Al_2Cu, $TiCu_3$, $Al_{4.2}Cu_{3.2}Zn_{0.7}$, $Al_{0.71}Zn_{0.29}$, Ti_2Cu, Al_3Ti, and $TiZn_{16}$"[12] IMCs were formed at the bonding interface. Anbarzadeh et al.[14] analyzed the effects of successive-stage TLP on metallurgical and tensile properties of Al2024–Ti6Al4V joints. It is revealed that good bonding was achieved by employing Sn-based alloy as insert material with a tensile strength of 62 MPa. The following intermetallic phases Ag_3Al, Ag_2Al, and Al_3Ti were formed at the interface and Sn as solid solution bonding. The tensile shear strength is directly related to BT. The longer the BT higher will be the shear strength.[12,39,96] Winiowski and Majewski[97] studied the effect of Ag as insert material on the metallurgical and tensile properties of TLP bonding of grade 2 Ti-6082 alloy. High-quality joints are obtained with high shear strength 20 MPa (because of the existence of TiAl, Ti_5Al_{11}, $AlTi_3$, and Al_3Ti IMCs) at 530°C braze temperature and HT of 30 min. It is found that joint strength gets reduced when increasing braze temperature and holding time.

Brazing. In this method, an interlayer or solder is added from outside between the braze materials. By using suitable diffusive treatment of the melted solder and joined materials, the brazed joint is produced according to the isothermal solidification process.[99] A schematic diagram showing stages of the brazing process as explained in Figure 28. The brazing process consists of the following six stages namely joint design, cleaning, oxidation removal, heating,

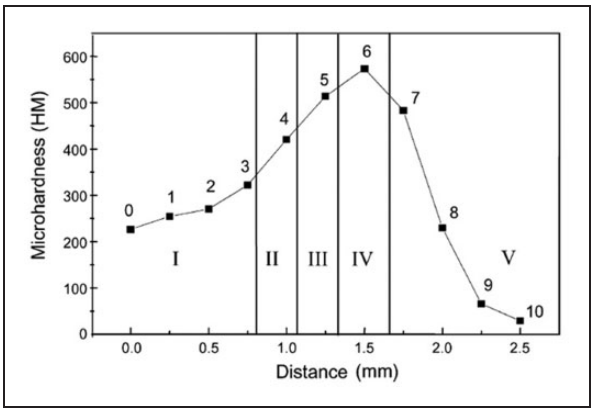

Figure 25. Microhardness distribution at the interface zone of Ti–Al diffusion bonding.[33]

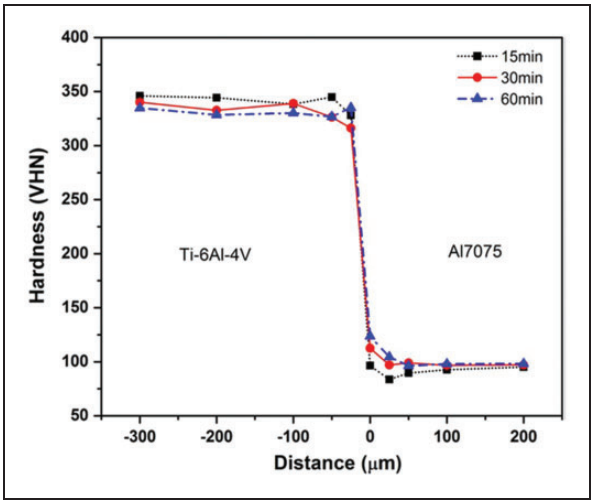

Figure 27. Diffusion zone microhardness at different bonding times.[39]

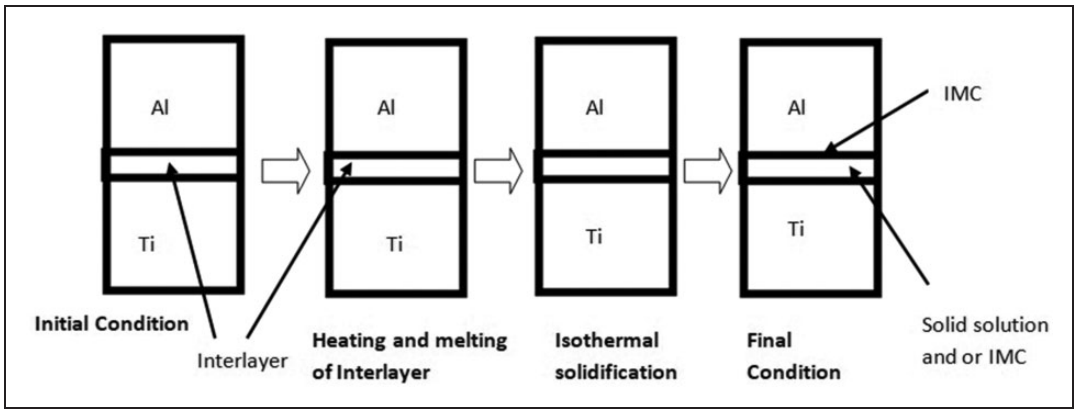

Figure 26. Schematic of the transient liquid phase bonding process.
IMC: intermetallic compounds.

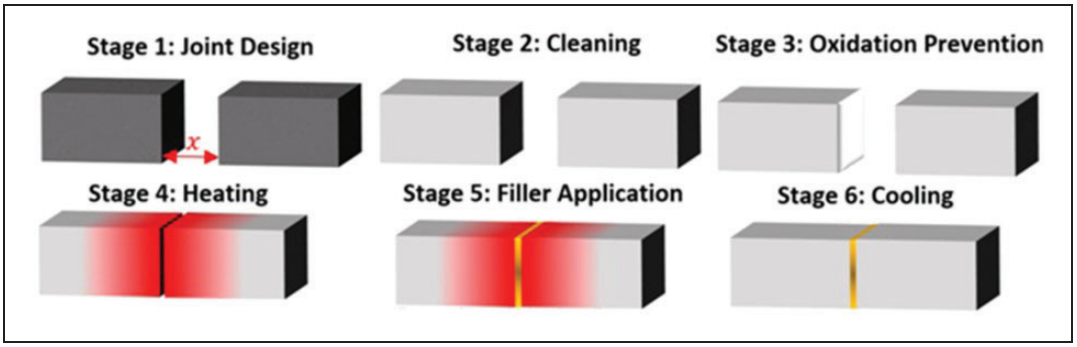

Figure 28. Schematic diagram showing stages of the brazing process.[105]

application of filler, and cooling. In the first stage, the components are arranged with a gap and are corrected at brazing temperature due to thermal expansion. In the second stage, the components are properly cleaned to remove grease, dirt, and surface oxides. The oxide layer is then removed by applying flux or by performing brazing operation in a vacuum or reducing atmosphere. The components are heated to the brazing temperature by employing suitable jigs. Then the filler metal is applied and is gets filled into the joint due to capillary action. Different forms of filler metal either foil or paste can be applied directly into the joint before heating. Lastly, the assembly is cooled and any flux residue (if used) is removed using a suitable cleaning method.[105]

Suslov[106] developed a technology consisting of brazing three-layer panels with a honeycomb filler for light alloys based on Ti and Al in vacuum furnaces. The process not only improves the geometrical parameters of brazed sections but also reduces the labor content, and improves the quality of brazed joints than brazing panels in containers.

Chang et al.[98] examined the influence of rare earth materials in the brazing of 6061-Ti6Al4V alloys. It is revealed that the rare-earth element which not only lowers the interfacial reaction energy but also reduces the solidus and liquidus temperatures. The results indicate that a ternary $Al_5Si_{12}Ti_7$ IMC phase formed at the Al alloy filler metal/Ti6Al4V brazed with the $Al_{8.4}Si_{20}Cu_{10}Ge_{0.1}Re$ filler metal interface. Nesterov et al.[107] investigated Ti brazed with an Al brazing alloy joint formation considering wetting the surface and brittle intermetallic interlayer formation. To control the wetting process, it is desirable to reduce the partial pressure of oxygen in brazing. It is observed that 0.16 to 0.22 μm/s high growth rate of Al_3Ti IMCs.

Winiowski and Różański[99] studied the effect of different interlayers in diffusive brazing (which is a hybrid variant of diffusive welding and brazing) of Ti and its alloys with Al. They have considered three interlayers as B-Ag72Cu-780-type silver solder foil, copper (Cu), and nickel (Ni) for diffusive brazing of Ti grade 2 and TiAl (γ) phase matrix. It is revealed that due to very low joint strength, Ni interlayer for Ti-diffusive brazing as well as Cu and Ni interlayers for $TiA1_{48}Cr_2Nb_2$ (γ) alloy brazing was not applied.

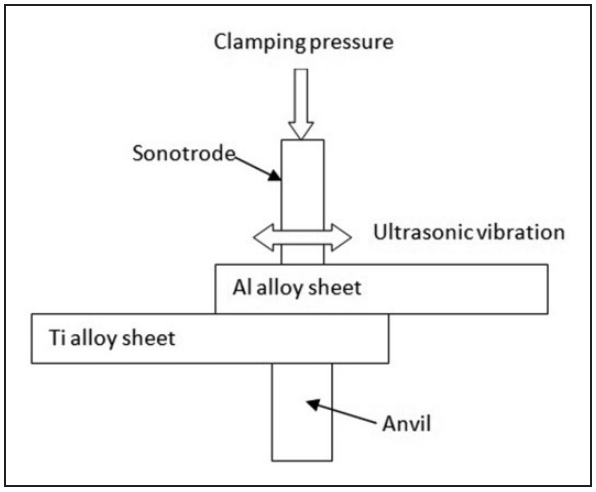

Figure 29. Schematic diagram showing the ultrasonic welding process.

Ultrasonic welding. It is a solid-state welding process wherein the joint is produced by ultrasonic vibrations is applied to the pieces to be joined being held together under pressure as explained in Figure 29. Zhu et al.[27] investigated the influence of ultrasonic welding process variables on the weld interface properties of AA6061–Ti6Al4V alloys. It can be seen that a joint of these materials effectively bonded and achieved the strongest joint at 0.4 MPa welding pressure and 170 ms welding time. The interface matrix hardness improved in contrast with the base metal, especially around the weld interface region. The diffusion layer width is directly related to welding time.

Zhang et al.[15] investigated the metallurgical and tensile properties of Al6061–Ti6Al4V alloys using pure Al-particle as interlayer via ultrasonic spot welding (USW). The joint shear strength increased ~106 MPa at 1100 J welding energy, with increasing weld energy the failure mode changed from interfacial to pull-out mode. It is revealed that no IMCs formed at the interface of a joint of pure Al insert material with Ti alloy. Al6061 alloy has a better hardness in the bond area, while the Ti6Al4V alloy hardness

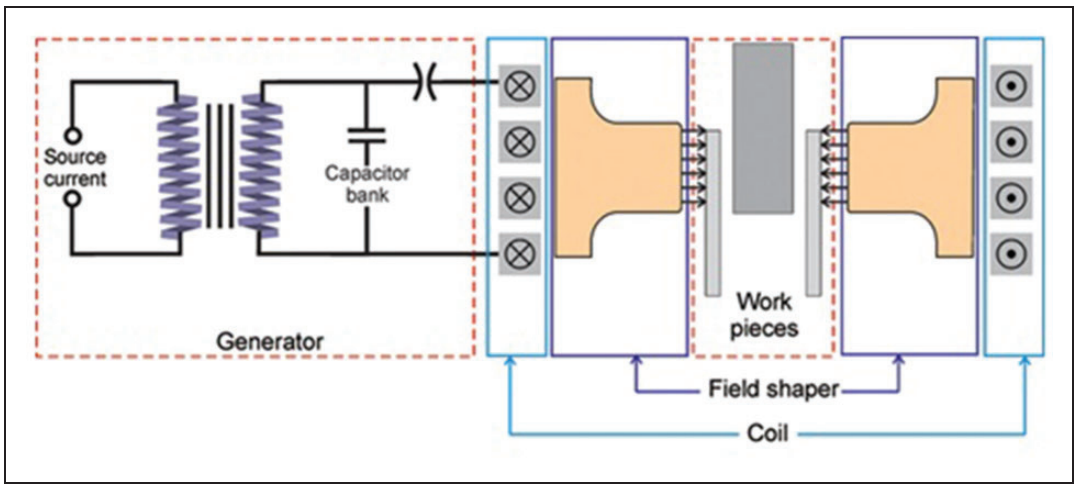

Figure 30. Schematic diagram showing a principle of magnetic pulse welding.[108]

remains unchanged after welding. Zhang et al.[100] examined the possibility of high power USW of AA2139 to TiAl6V4 alloy and investigated the microstructure, mechanical property, and weld thermal cycle. It is claimed that the highest shear strength of ~100 MPa achieved which is superior to other different material groups, e.g. Al–Mg and Al–Fe due to the absence of IMC formation in the case of Al–Ti. No apparent IMC layer was found in AA2139/TiAl6V4 joints of USW. Zhou et al.[43] studied the metallurgical properties of the AA6061 Al alloy and cp Ti alloy by USW. They do not find any IMC or major IMC layer formation, even at the highest weld time of 1.4 s. Increasing the weld time, the maximum joint load first enhanced with the increase of bond region, then reduced because of fatigue crack observed in the Al side. Balle and Magin[101] optimized process parameters of Al4N, AA7075, cp Ti, and TiAl6V4 using ultrasonic welding. The microstructural results showed that the joining zone, which is formed as a function of the applied oscillation amplitude and the radius of the sonotrode coupling face. The weld formation takes place in the range of ~230°C for Al4N/cp Ti joints.

Pressure welding. Iwamoto et al.[29] pressure welding of Al to Ti successfully joined Al to Ti using pressure welding with the Al layer was coated to Ti before welding. Due to this Al layer, the joint is possible in the air at elevated temperature with Al_3Ti as IMC formed in the weld. The joint showed maximum strength when welded in 200–350°C beyond which it decreases due to oxidation or softening of Al.

Electromagnetic or magnetic pulse welding. It is a solid-state welding process wherein magnetic forces are utilized for the pieces to be joined. The principle of operation of the magnetic pulse welding (MPW) process is depicted in Figure 30. Marya et al.[103] studied the characteristics of electromagnetic welds of Al and Ti alloys. It is revealed that mechanical interlocking (which is produced because of plastic deformation and microcracks at the surface of each material) and new intermetallic phases are the main factors for deciding the electromagnetic pulse welding (EMW) joints. Psyk et al.[104] successfully joined Al99.5 and titanium TiAl6V4 alloys using EMW by varying impact velocities. An optimum impact velocity of 100 m/s was obtained for a 5° impact angle. It can be seen that an extremely thin transition area between Al–Ti alloys is advantageous to the fusion-based processes.

Explosive welding or cladding. The joining mechanism of explosive welding is almost similar to that of the MPW process. Kahraman et al.[109] analyzed the metallurgical, tensile properties, and corrosion resistance in seawater of the explosively joined Ti6Al4V and Al plates at various explosive loads. There is no peeling found in the interface after the tensile-shear test. Mass variations were observed at different explosive loads shown in Figure 31. The defect-free joints with no IMCs and melting cavities (pores) were seen at the interface with maximum hardness near the interface area. At the beginning of the corrosion test, the loss of mass in welded samples was rapid and was continued at a slower rate and the amount of corrosion was increased with explosive load addition due to internal stress. Fronczek et al.[16] examined the metallurgical and tensile properties of Ti (Ti Gr.2)/Al (A1050) clads fabricated using explosive welding and annealing. After the explosion, defect-free welds were observed and Al_3Ti, $TiAl_2$, TiAl, and Ti_3Al intermetallic phases were found within the vortex, where the Al_3Ti phase was dominant after annealing. It is suggested that this dissimilar material combination can also be suitably used for fabricating metallic–intermetallic laminate (MIL) composites.

Gurevich et al.[110] investigated the structural inhomogeneities of Ti–Al composite, produced via explosive welding. It is observed that titanium aluminide particles in the matrix of the Al-based solid solution

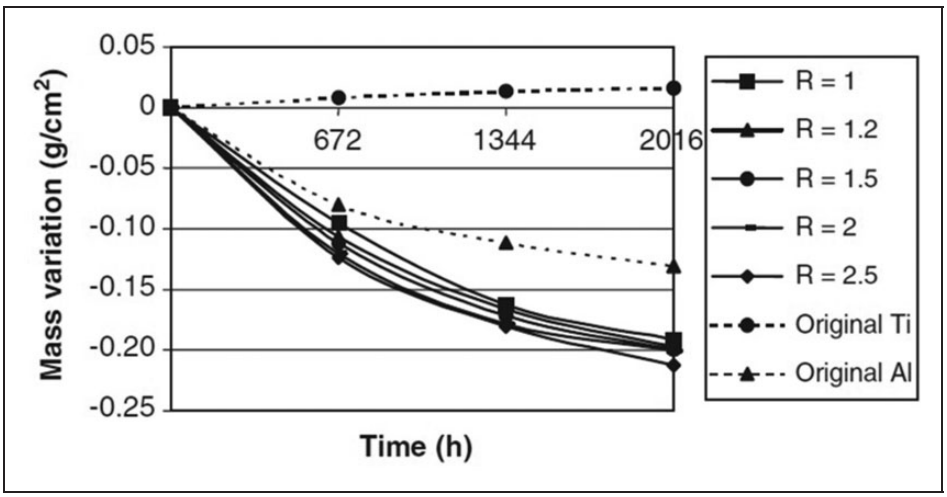

Figure 31. Mass variations for Al–Ti composites using explosive welding at different explosive loads (R) in the corrosion test.[109]

were formed in the local heterogeneous molten areas. Trykov et al.[111] studied the cold rolling of the explosion-welded three-layer Ti–Al composite joints (AMg-CADl-VT1). It is observed a non-uniform longitudinal and transverse deformation which depends on compression and the strength characteristics ratio of the welded metals.

Accumulative roll bonding. It is a severe plastic deformation (SPD) rolling process wherein similar or dissimilar metal sheets are repeatedly rolled to severe reduction, sectioning, again piling, and rolling that resulted in the production of ultrafine grain structure material. A schematic diagram of the accumulative roll bonding process is explained in Figure 32. Maier et al.[112] studied the nanomechanical behavior of Al–Ti film layer matrices fabricated using accumulative roll bonding (ARB). A rolled 100 μm Ti-foils into two 1 mm cp AA1050 sheets was employed using the ARB process with Ti foil inside and two Al sheets outside. It is observed that at 180° and 400° annealing temperatures a poor bonding with surface flaws produced, while at 600°C an interdiffusion region arises that consists of small phases of the Al_3Ti intermetallic phase. Ng et al.[113] analyzed the effect of roll diameter ratio on microstructural evolutions of the Al/Ti composite sheets processed by asymmetric ARB. It is found that the ductility and joint strength improves with an increase in the ratio of roll diameter. Further, the grain refinement of the Al matrix along with a nanostructured surface deposit on Ti (50–100 nm) produced which is lacking in symmetric ARB. Similarly, a 15% increase in the interdiffusion layer was produced in asymmetric ARB than symmetric ARB.

To conclude, the DB processes was claimed low shear strength than the FSSW of dissimilar joints of Al–Ti alloys. The differences in the strength of both processes are attributed due to the joining

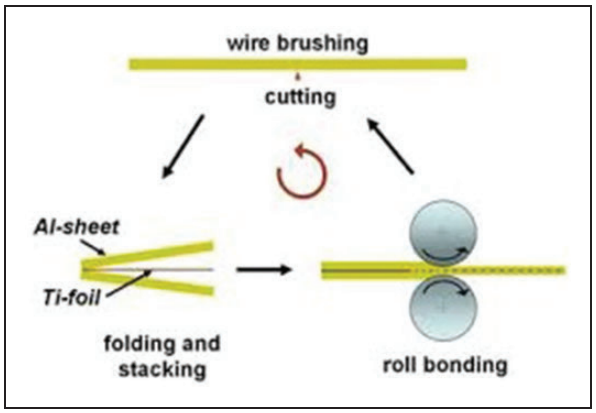

Figure 32. Schematic diagram showing the accumulative roll bonding process.[112]

mechanism. In friction-based processes, the joints are produced by friction (shoulder) and material deformation (tool pin), whereas in diffusion bonding processes the joints are produced by the application of heat and pressure at the finite interval (diffusion). The joint shear strength is a function of bonding temperature and holding time. On the contrary, the bonding pressure has less effect on the joint shear strength than the bonding temperature and the holding time. The maximum shear strength of dissimilar joints of Al–Ti alloys using the TLP bonding process is reported using Sn-based alloy as insert material. Similarly, maximum shear strength using the USW process is claimed using pure Al insert material with no IMC formation. The other welding processes like brazing, ultrasonic welding, pressure welding, EMW/MPW, explosive welding or cladding, and ARB processes have not fully explored that can be explored by considering their underlying physics along with each of the process parameters or their hybrid approaches.

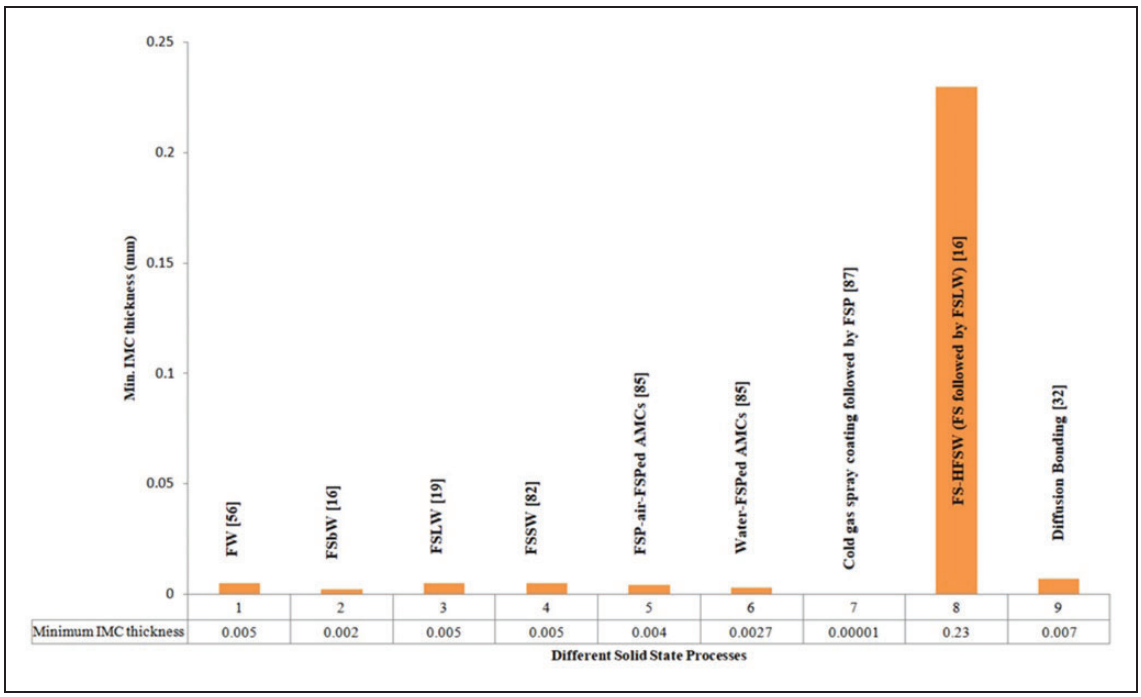

Figure 33. Minimum IMC thickness among different solid-state welding processes.
FW: friction welding; FSbW: friction stir butt welding; FSLW: friction stir lap welding; FSSW: friction stir spot welding; FSP: friction stir processing; AMC: aluminum matrix composite; FS-HSFW: friction surfacing followed by friction stir lap welding.

Minimum IMC thickness among different solid-state welding processes

During welding processes of Al–Ti joints, the welding heat input influenced the microstructural evolution, especially IMCs. Figure 33 shows the summary of the minimum IMC thickness produced in different solid-state welding processes, which determined the joint strengths. It is claimed that the critical IMC layer thickness ~ 5 μm able to produce high-quality FW joints.[54]

Tensile strength comparison among different solid-state welding processes

A statistics for tensile properties of Al–Ti joints by different solid-state welding processes are explained in Tables 6 and 7. It can be seen from Table 6 that the tensile strength (TS) in the case of the FW process nearly the same with or without interlayer. In the case of FSbW of cp Al and cp Ti, the TS relatively increased (TS: 138 MPa) using Zn interlayer, which hinders the formation Al_3Ti IMC layer in contrast to without interlayer.[24] On the contrary, using the Nb interlayer, the TS decreased to 66 MPa owing to the defect formation in the weld zone than without the interlayer having TS of 117 and 97 MPa.[19] TPO has a strong influence on the interfacial microstructures and mechanical properties of joints. Too small or too large TPO resulted in no bonding or large IMC formed at the interface. It is recommended to keep TPO on Al side to get sound joints.[12,14–16,24–27,29,31,33,35,36] In addition to this, Zn insert layer with different TPOs in the FSW process revealed that the TPO position restricts the number of ternary materials mechanical mixing (TS: 132 MPa at TPO: 1.6 mm).[61] Similarly, using different TPO with Cu interlayer in FSW process, higher hardness values were achieved at lowest TPO, whereas with more TPO weld defects are formed.[20] In underwater FSP, the highest YS (265 MPa) and UTS (423 MPa) is achieved with the ductility of 15% than air FSP.[85] Cooling-assisted FSW (CFSW) has reported better mechanical properties with the highest joint efficiency (42% of AA6061), TS: 120 MPa (finer grains) than normal FSW (NFSW), and heating assisted (HFSW where large-sized grains produced due to slow cooling). This is due to rapid cooling rates.[60]

The new approaches of FSW like UaFSW and GTAWaFSW showed much of the improvement in the TS from 215 MPa (FSbW) to 236 MPa (UaFSW) and 300 MPa (GTAWaFSW) for the AA6061-T6–Ti6Al4V alloy combination. The UaFSW process enhances the strength of the joint. The strength of the weld decreases with too large amplitude or pressure, causing weld inner defects. The process performs better in lap-shear condition than conventional FSLW.[38]

It can be seen from Table 7 that the shear strength of AA2024-Ti6Al4V alloy joining using TLP bonding process with Sn–5.3Ag–4.2Bi as an interlayer is almost double than Cu – 22%Zn interlayer. Similar results are also seen for AA7075–Ti6Al4V alloy with Sn–4Ag–3.5Bi as an interlayer than the Cu interlayer.

Table 6. Tensile strength of different solid-state welding processes.

Processes	TS	Interlayer	Al–Ti grade	Ref.	Remark
FW	186.59 MPa	–	AA6061-T6–Ti6Al4V	2	–
	189.92 MPa	Electrodeposited Zn	Ti6Al4V–AA6061	56	–
FSbW	97 MPa	–	Pure Ti and pure Al	5	–
	117 MPa	–	cp Al to cp Ti	9	–
	66 MPa	Nb	cp Al to cp Ti	11	–
	311 MPa	–	Ti6Al4V–AA2024-T3	13	–
	201 MPa	–	Ti6Al4V–AA7075-T651	13	–
	197 MPa	–	Ti6Al4V–AA6061-T6	14	–
	215 MPa	–	Ti6Al4V–AA6061-T6	15	–
	292 MPa	–	Ti6Al4V-Al–6Mg	16	–
	134 MPa	–	Ti6Al4V–AA6061-T6	17	–
	138 MPa	Zn	cp Al to cp Ti	24	–
	271 ± 6 MPa	–	Ti6Al4V–AA2024-T3	25	2nd pass
	231 ± 6 MPa	–	Ti6Al4V–AA2024-T3	25	1st pass
	265 MPa	–	Ti6Al4V–5A06 Al	41	–
	348 ± 7.67 MPa	–	TiAl6V4–AA2024-T3	42	–
	120 MPa	–	Pure Ti and AA6061-T651	61	Water cooling
	132 MPa	Zn	cp Al to cp Ti	62	
	131.1 MPa	–	TC1 Ti alloy – LF6 Al	63	–
	142.97 MPa	–	AA6061–Ti	64	–
FSP	383 ± 4 MPa	–	AA5083–pure Ti powder	85	Air
	423 ± 7 MPa	–	AA5083–pure Ti powder	85	Water-FSP
	193.1 ± 3 MPa	–	AA5052 as-cast–TiO_2 powder	86	–
UaFSW	236 MPa	–	AA6061-T6–Ti6Al4V (TC4)	3	–
GTAWaFSW	300 MPa	–	AA6061-T6–Ti6Al4V	88	–

FW: friction welding; FSbW: friction stir butt welding; FSP: friction stir processing; UaFSW: ultrasonic-assisted friction stir welding; GTAWaFSW: gas tungsten arc welding-assisted friction stir welding.

Table 7. Shear strength of different solid-state welding processes.

Processes	SS	Interlayer	Al–Ti grade	Ref.	Remark
FSLW	147 MPa	–	AA6061-T6–Ti6Al4V	18	-
	9.39 kN	–	ADC12 cast Al-pure Ti	19	Max. failure load
	~8.5 kN	–	Pure Al–Ti6Al4V (multi-pass)	21	Max. failure load
	4500 N	–	AA6061–Ti6Al4V	31	Max. failure load
	147.5 MPa	–	AA6061–Ti6Al4V	35	-
	200 N/mm	–	Ti6Al4V–AA2024-T4	74	Max. failure load
	1910 N	–	AA1060–Ti6Al4V	75	Max. failure load
	2.8 kN	–	TC1–LF6 Al	76	Max. failure load
	4026 N	–	AA6061–Ti6Al4V	79	Max. failure load
FSSW	6449 ± 554 N	–	AA6181-T4–Ti6Al4V	36	Lap shear force
	7.4 kN	–	AA5754–Ti6Al4V	82	Max. shear load
	4.2 kN	–	AA6061–Ti6Al4V	84	Max. shear load
FMSW	18.2 kN	–	2A12-T4–Ti6Al4V	22	Max. shear load
Diffusion bonding	87 MPa	–	cp–Ti/AA7075	32	–
Diffusive brazing	264–303 MPa	B–Ag72Cu-780, CF032A, Ni99.0	Ti Grade 2–$TiAl_{48}Cr_2Nb_2$	98	–
TLP bonding	37 MPa	Cu – 22%Zn	AA2024–Ti6Al4V	4	–
	62 MPa	Sn–5.3Ag–4.2Bi	AA2024–Ti6Al4V	6	–
	36 MPa	Sn–4Ag–3.5Bi	AA7075–Ti6Al4V	39	–
	19.5 MPa	Cu	AA7075–Ti6Al4V	95	–
	20 MPa	Ag72Cu28	AA6082–Ti Grade 2	96	–
Ultrasonic welding	106 MPa	Pure Al interlayer	AA6061–Ti6Al4V	7	–
Ultrasonic spot welding	~100 MPa	–	AA2139-T8–Ti6Al4V	99	–
Ultrasonic torsion welding	41.4 ± 3.7 MPa	–	AA7075-T6–Ti6Al4V	100	–
	15.2 ± 0.5 MPa	–	Al4N–cp–Ti	100	–
	15.2 ± 0.5 MPa	–	AA1199–cp–Ti	101	–

FSLW: friction stir lap welding; FSSW: friction stir spot welding; FMSW: friction melt-bonded spot welding; TLP: transient liquid phase bonding.

The effect of WS on FSLW of AA6061 and Ti6Al4V has been studied and revealed a maximum shear load of 4026 N, which is attributed due to a small Al_3Ti IMC layer formed at WS 80 mm/min.[79] A medium interface thickness of 7.5 μm attained for the maximum shear load of 4500 N at TRS of 1000 r/min and WS 100 mm/min. Too small or too large interface thickness resulted in weak bond or excessive IMCs formation that leads to poor shear strength.[31] Further, the probe length has more influence on the interfacial microstructure and mechanical properties of Al–Ti lap joints. Maximum shear strength is revealed for 3.1 mm probe length (shear strength: 147.5 MPa).[35] In FSSW, low TRS and low dwell time reported maximum tensile shear load (4.2 kN) due to the formation of Ti-rich $AlTi_3$ IMC.[84]

In USW, it is revealed that too large or too small welding time is not recommended due to poor mechanical properties of the joints.[43] Maximum tensile shear strength of 5128 N is reported at a welding time of 1 s. The use of pure Al particle as an interlayer in USW gives the lap shear strength 52.5% higher than without interlayer.[15] In the TLP process, the hardness of the joint interface increases when BT increases, which are attributed to the IMC formation. An increase in BT increases the bond strength and reaches to a maximum of 36 MPa at 60 min with the formation of TiAl and $AlTi_3$ IMC.[39]

Common defects observed and their prevention in joining Al–Ti alloys

The formation of defects in friction-based processes occurs due to insufficient HI or improper selection of process parameters like tool TA, TRS, WS, or TPO in case of the FSW process; RS, FP, FT, UP, UT, etc. in case of FW process.

There are no appreciable defects found for FW, DB process in the literature. However, FSW and its variants claimed surface grooves, macro- and micro-cracks, tunnels, voids, surface galling, wormhole, excessive flash, nugget collapse, etc.;[40] voids[97] found in case of diffusion brazing. The above-mentioned defects can be reduced or eliminated with sufficient HI, properly selected process parameters, tool design, hybrid processes.

Missing researches for future work

From the above sections, it is evident that the solid-state joining process is a viable process for welding Al–Ti alloys. However, still some of the important issues that need to be addressed to get a commercially acceptable joint. Firstly, the welding of Al–Ti alloys is a complex issue. However, many of the parameters not considered yet can be explored in the above-mentioned processes like joint geometry and design, different interlayers with different sizes, the influence of other process parameters, etc. Since the majority of the referred literature is based on FSW and their allied processes, hence this section deals with these processes with future research directions. During FSW, the rotating tool contacted with the Ti alloys, which resulted in the tool erosion. The related design of welding tools is essential, the efforts can be extended to employ the concept of friction surfacing assisted friction stir lap welding,[114] friction stir diffusion bonding,[115] friction stir scribe welding technique,[116] circumferential notches probe shape tool,[117,118] and Bobbin tool friction stir welding.[119] It is recommended that before FSLW of Al–steel joints, the Al coating is first applied on the steel using friction surfacing to avoid tool wear and to reduce IMCs. It is ascertained that circumferential notches probe shape eliminated the general defects, probe abrasion, large metallurgical bond area, and high joint strength.[117] Furthermore, some of the inherent problems that occur during conventional FSW must be solved like the reduction of the fixture complexity and the lack of root penetration defect avoidance. Increase in the effective load-bearing area and elimination of stress concentration. Keyhole repairing and other defects and retain approximately equal strength after remanufacturing.[120]

Similarly, as of now, only a few of the processes have been studied thoroughly, significant efforts are needed to explore other solid-state processes by considering different process parameters, joint design, its geometry. In self-riveting FSW of Al–steel lap joints, the combined effect of mechanical and metallurgical bonding the joint strength is significantly improved[121,122] where the equidistance prefabricated holes were produced in steel sheet and the plasticized Al gets filled in these holes. It is claimed that lap FSW joint strength achieved 23% more than the conventional FSW process. Such concepts can be explored to join Al–Ti. Secondly, for making a state-of-the-art[123] process, a clear understanding of the thermomechanics of these solid-state welding processes is essential by which the mathematical models can be developed. These models as an input to the different efficient algorithms in which the process parameters can be optimized efficiently with multiple inputs to get commercially acceptable welds. Finally, expert systems can be developed based on existing data of Al–Ti alloys, which will be a ready reckoner for the welder or practitioner. The expert systems along with a digital twin, cloud computing, or fog/edge computing platform will give a roadmap towards Industry 4.0 for different solid-state and its related hybrid welding processes for joining of dissimilar Al–Ti alloys.

Conclusion

In this article, different solid-state and their related hybrid welding processes have been discussed for the welding of different Al alloys with Ti alloys. The paper reviews the reported literature based on process

variables, tool design, and material on the microstructural and mechanical properties. The brittle intermetallic phase formation reduces joint strength. These phases are produced due to extreme HI. However, their formation is inevitable but can be restricted by proper selection of process parameters, tool design, and offset. The review showed that literature lacks to formulate the other process conditions for each of the processes to get commercially acceptable welds. The joint efficiencies are varied for different welding processes; it is in case of friction welding: 100%, FSbW: ~94% of Al, FSLW: 71%, water FSP: ~204% of Al, FS-HFSW: 85.3% of Al, UVaFSLW: 200%, UaFSW: 85% of Al, GTAWaFSW: 91% of Al, DB: 42%, TLP bonding: ~30% of Al, ultrasonic welding: 51.2% of Al, etc. Other solid-state welding processes that have not been explored so far can be explored for Al–Ti welding. The efforts can be made to achieve this through weld analysis and simulation, exploitation of optimization techniques, or machine learning algorithms to make process window to get defect-free welds, expert systems that will be a ready reckoner for the welder or practitioner. The expert systems along with different computing platforms will give a roadmap towards Industry 4.0 for each of the processes for joining dissimilar Al–Ti alloys.

Acknowledgments

The authors are extremely thankful to the Editor and the referees for their valuable comments and suggestions, which contributed significantly to improve the quality of the paper.

Declaration of conflicting interests

The author(s) declared no potential conflicts of interest with respect to the research, authorship, and/or publication of this article.

Funding

The author(s) disclosed receipt of the following financial support for the research, authorship, and/or publication of this article: The first author wishes to express his deep thanks and appreciation to All India Council for Technical Education (AICTE), New Delhi for providing financial support under the research promotion scheme project no. 8-117/FDC/RPS (Policy-1)/2019-20.

ORCID iD

Vijay S Gadakh https://orcid.org/0000-0002-9172-261X

References

1. Kimura M, Nakamura S, Kusaka M, et al. Mechanical properties of friction welded joint between Ti–6Al–4V alloy and Al–Mg alloy (AA5052). *Sci Technol Weld Join* 2005; 10: 666–673.
2. Hynes NRJ and Velu PS. Effect of rotational speed on Ti-6Al-4V-AA 6061 friction welded joints. *J Manuf Process* 2018; 32: 288–297.
3. Aonuma M and Nakata K. Dissimilar metal joining of 2024 and 7075 aluminium alloys to titanium alloys by friction stir welding. *Mater Trans* 2011; 52: 948–952.
4. Bang KS, Lee KJ, Bang HS, et al. Interfacial microstructure and mechanical properties of dissimilar friction stir welds between 6061-T6 aluminum and Ti-6% Al-4% V alloys. *Mater Trans* 2011; 52: 974–978.
5. Yu M, Zhao H, Jiang Z, et al. Influence of welding parameters on interface evolution and mechanical properties of FSW Al/Ti lap joints. *J Mater Sci Technol* 2019; 35: 1543–1554.
6. Chen YC and Nakata K. Microstructural characterization and mechanical properties in friction stir welding of aluminum and titanium dissimilar alloys. *Mater Des* 2009; 30: 469–474.
7. Li B, Shen Y, Luo L, et al. Fabrication and anti-oxidation properties of Al/Ti-6Al-4V bimetallic clad-sheet by multi-pass friction stir welding. *Proc IMechE, Part B: J Engineering Manufacture* 2015; 229: 1078–1082.
8. Li B, Shen Y, Luo L, et al. Effects of processing variables and heat treatments on Al/Ti-6Al-4V interface microstructure of bimetal clad-plate fabricated via a novel route employing friction stir lap welding. *J Alloys Compd* 2016; 658: 904–913.
9. Chen Y, Deng H, Liu H, et al. A novel strategy for the reliable joining of Ti6Al4V/2A12-T4 dissimilar alloys via friction melt-bonded spot welding. *Mater Lett* 2019; 253: 306–309.
10. Huang Y, Lv Z, Wan L, et al. A new method of hybrid friction stir welding assisted by friction surfacing for joining dissimilar Ti/Al alloy. *Mater Lett* 2017; 207: 172–175.
11. Ma Z, Jin Y, Ji S, et al. A general strategy for the reliable joining of Al/Ti dissimilar alloys via ultrasonic assisted friction stir welding. *J Mater Sci Technol* 2019; 35: 94–99.
12. Samavatian M, Khodabandeh A, Halvaee A, et al. Transient liquid phase bonding of Al 2024 to Ti-6Al-4V alloy using Cu-Zn interlayer. *Trans Nonferrous Met Soc China (English Ed)* 2015; 25: 770–775.
13. Choi JW, Liu H and Fujii H. Dissimilar friction stir welding of pure Ti and pure Al. *Mater Sci Eng A* 2018; 730: 168–176.
14. Anbarzadeh A, Sabet H and Abbasi M. Effects of successive-stage transient liquid phase (S-TLP) on microstructure and mechanical properties of Al2024 to Ti-6Al-4V joint. *Mater Lett* 2016; 178: 280–283.
15. Zhang HM, Chao YJ and Luo Z. Effect of interlayer on microstructure and mechanical properties of Al–Ti ultrasonic welds. *Sci Technol Weld Join* 2017; 22: 79–86.
16. Fronczek DM, Wojewoda-budka J, Chulist R, et al. Structural properties of Ti/Al clads manufactured by explosive welding and annealing. *Mater Des* 2016; 91: 80–89.
17. Kar A, Suwas S and Kailas SV. Multi-length scale characterization of microstructure evolution and its consequence on mechanical properties in dissimilar friction stir welding of titanium to aluminum. *Metall Mater Trans A Phys Metall Mater Sci* 2019; 50: 5153–5173.
18. Kar A, Suwas S and Kailas SV. Microstructural modification and high-temperature grain stability of

aluminum in an aluminum-titanium friction stir weld with zinc interlayer. *JOM* 2019; 71: 444–451.
19. Kar A, Choudhury SK, Suwas S, et al. Effect of niobium interlayer in dissimilar friction stir welding of aluminum to titanium. *Mater Charact* 2018; 145: 402–412.
20. Kar A, Suwas S and Kailas SV. Significance of tool offset and copper interlayer during friction stir welding of aluminum to titanium. *Int J Adv Manuf Technol* 2019; 100: 435–443.
21. Song Z, Nakata K, Wu A, et al. Influence of probe offset distance on interfacial microstructure and mechanical properties of friction stir butt welded joint of Ti6Al4V and A6061 dissimilar alloys. *Mater Des* 2014; 57: 269–278.
22. Wu A, Song Z, Nakata K, et al. Interface and properties of the friction stir welded joints of titanium alloy Ti6Al4V with aluminum alloy 6061. *Mater Des* 2015; 71: 85–92.
23. Li B, Zhang Z, Shen Y, et al. Dissimilar friction stir welding of Ti-6Al-4V alloy and aluminum alloy employing a modified butt joint configuration: influences of process variables on the weld interfaces and tensile properties. *Mater Des* 2014; 53: 838–848.
24. Kar A, Kailas SV and Suwas S. Effect of zinc interlayer in microstructure evolution and mechanical properties in dissimilar friction stir welding of aluminum to titanium. *J Mater Eng Perform* 2018; 27: 6016–6026.
25. Kar A, Suwas S and Kailas SV. Two-pass friction stir welding of aluminum alloy to titanium alloy: a simultaneous improvement in mechanical properties. *Mater Sci Eng A* 2018; 733: 199–210.
26. Vaidya W V, Horstmann M, Ventzke V, et al. Structure-property investigations on a laser beam welded dissimilar joint of aluminium AA6056 and titanium Ti6Al4V for aeronautical applications, Part I : local gradients in microstructure, hardness and strength. *Materwiss Werksttech* 2009; 40: 623–633.
27. Zhu Z, Lee KY and Wang X. Ultrasonic welding of dissimilar metals, AA6061 and Ti6Al4V. *Int J Adv Manuf Technol* 2012; 59: 569–574.
28. Moller F, Thomy C and Vollertsen F. Joining of titanium-aluminium seat tracks for aircraft applications – system technology and joint properties. *Weld World* 2012; 56: 108–114.
29. Iwamoto N, Tabata S and Takeuchi T. Pressure welding of aluminum to titanium. *Trans JWRI* 1976; 5: 63–66.
30. Meisnar M, Baker S, Bennett JM, et al. Microstructural characterisation of rotary friction welded AA6082 and Ti-6Al-4V dissimilar joints. *Mater Des* 2017; 132: 188–197.
31. Yu M, Zhao H, Jiang Z, et al. Microstructure and mechanical properties of friction stir lap AA6061-Ti6Al4V welds. *J Mater Process Technol* 2019; 270: 274–284.
32. Rajakumar S and Balasubramanian V. Diffusion bonding of titanium and AA 7075 aluminum alloy dissimilar joints—process modeling and optimization using desirability approach. *Int J Adv Manuf Technol* 2016; 86: 1095–1112.
33. Jiangwei R, Yajiang L and Tao F. Microstructure characteristics in the interface zone of Ti/Al diffusion bonding. *Mater Lett* 2002; 56: 647–652.
34. Rostami H, Nourouzi S and Jamshidi Aval H. Analysis of welding parameters effects on microstructural and mechanical properties of Ti6Al4V and AA5052 dissimilar joint. *J Mech Sci Technol* 2018; 32: 3371–3377.
35. Zhao H, Yu M, Jiang Z, et al. Interfacial microstructure and mechanical properties of Al/Ti dissimilar joints fabricated via friction stir welding. *J Alloys Compd* 2019; 789: 139–149.
36. Plaine AH, Suhuddin UFH, Alcântara NG, et al. Microstructure and mechanical behavior of friction spot welded AA6181-T4/Ti6Al4V dissimilar joints. *Int J Adv Manuf Technol* 2017; 92: 3703–3714.
37. Plaine AH, Gonzalez AR, Suhuddin UFH, et al. Process parameter optimization in friction spot welding of AA5754 and Ti6Al4V dissimilar joints using response surface methodology. *Int J Adv Manuf Technol* 2016; 85: 1575–1583.
38. Yu M, Zhao H, Xu F, et al. Influence of ultrasonic vibrations on the microstructure and mechanical properties of Al/Ti friction stir lap welds. *J Mater Process Technol* 2020; 282: 116676.
39. Kenevisi MS and Mousavi Khoie SM. An investigation on microstructure and mechanical properties of Al7075 to Ti-6Al-4V Transient Liquid Phase (TLP) bonded joint. *Mater Des* 2012; 38: 19–25.
40. Jain S, Bhuva K, Patel P, et al. A review on dissimilar friction stir welding of aluminum alloys to titanium alloys. In: Deb D and Balas VE (eds) *Innovations in infrastructure, advances in intelligent systems and computing*. Singapore: Springer, 2019, pp. 415–425.
41. Zhang Z, Li B, Feng X, et al. Friction-stir welding of titanium/aluminum dissimilar alloys: Joint configuration design, as-welded interface characteristics and tensile properties. *Proc IMechE, Part B: J Engineering Manufacture* 2014; 228: 1469–1480.
42. Dressler U, Biallas G and Alfaro Mercado U. Friction stir welding of titanium alloy TiAl6V4 to aluminium alloy AA2024-T3. *Mater Sci Eng A* 2009; 526: 113–117.
43. Zhou L, Min J, He WX, et al. Effect of welding time on microstructure and mechanical properties of Al-Ti ultrasonic spot welds. *J Manuf Process* 2018; 33: 64–73.
44. Vaidya W V, Horstmann M, Ventzke V, et al. Improving interfacial properties of a laser beam welded dissimilar joint of aluminium AA6056 and titanium Ti6Al4V for aeronautical applications. *J Mater Sci* 2010; 45: 6242–6254.
45. Kumar N, Yuan W and Mishra RSRS. *Friction stir welding of dissimilar alloys and materials*. Oxford: Butterworth-Heinemann, 2015.
46. Akinlabi ET and Akinlabi SA. Friction stir welding of dissimilar metals. In: Givi MKB and Asadi P (eds) *Advances in friction-stir welding and processing*. Cambridge: Woodhead Publishing, 2014, pp. 241–293.
47. Sujata M, Bhargava S, Suwas S, et al. On kinetics of TiAl3 formation during reaction synthesis from solid Ti and liquid Al. *J Mater Sci Lett* 2001; 20: 2207–2209.
48. Sujata M, Bhargava S and Sangal S. On the formation of TiAl 3 during reaction between solid Ti and liquid Al. *J Mater Sci Lett* 1997; 16: 1175–1178.
49. Givi MKB and Asadi P (eds). General introduction. In: *Advances in friction stir welding and processing*. Cambridge: Woodhead Publishing, 2014, pp. 1–18.

50. Fuji A and North TH. Influence of silicon in aluminium on the mechanical properties of titanium/aluminium friction joints. *J Mater Sci* 1995; 30: 5185–5191.
51. Fuji A, North TH, Ameyama K, et al. Mechanical properties of titanium-5083 friction joints. *Mater Sci Technol* 1997; 13: 673–678.
52. Fuji A, Ikeuchi K, Sato YS, et al. Interlayer growth at interfaces of Ti/Al – 1% Mn, Ti/Al – 4.6% Mg and Ti/pure Al friction weld joints by post-weld heat treatment. *Sci Technol Weld Join* 2004; 9: 507–513.
53. Fuji A. In situ observation of interlayer growth during heat treatment of friction weld joint between pure titanium and pure aluminium. *Sci Technol Weld Join* 2002; 7: 413–416.
54. Kim YC and Fuji A. Factors dominating joint characteristics in Ti - Al friction welds. *Sci Technol Weld Join* 2002; 7: 149–154.
55. Velu PS, Hynes NRJ and Vignesh NJ. Joining of AA 6061/Ti–6Al–4V with zinc interlayer using friction welding process. *J Brazilian Soc Mech Sci Eng* 2019; 41: 537.
56. Kim YC, Hayashi T, Fuji A, et al. Joint characteristics of dissimilar material friction welds (II) - in the case of Ti-Al welds (mechanics, strength and structural design). *Trans JWRI* 2000; 29: 91–96.
57. Hynes NRJ and Velu PS. Numerical simulation of friction welding of aluminium/titanium joints. *Mater Res Express* 2018; 6: 026573.
58. Fuji A, Ameyama K, Futamata M, et al. Effect of post - weld heat treatment on properties of commercially pure titanium/pure aluminium friction welds. Study of friction welding of titanium/aluminium (1st report). *Weld Int* 1994; 8: 638–645.
59. Mishra RS and Ma ZY. Friction stir welding and processing. *Mater Sci Eng R Reps* 2005; 50: 1–78.
60. Patel P, Rana H, Badheka V, et al. Effect of active heating and cooling on microstructure and mechanical properties of friction stir–welded dissimilar aluminium alloy and titanium butt joints. *Weld World* 2020; 64: 365–378.
61. Kar A, Kailas SV and Suwas S. Effect of mechanical mixing in dissimilar friction stir welding of aluminum to titanium with zinc interlayer. *Trans Indian Inst Met* 2019; 72: 1533–1536.
62. Chen Y, Liu C and Liu G. Study on the joining of titanium and aluminum dissimilar alloys by friction stir welding. *Open Mater Sci J* 2011; 5: 256–261.
63. Patel S, Fuse K, Gangvekar K, et al. Multi-response optimization of dissimilar Al-Ti alloy FSW using Taguchi-Grey relational analysis. *Key Eng Mater* 2020; 833: 35–39.
64. Ghogheri MS, Asgarani KM and Amini K. Friction stir welding of dissimilar joint of aluminum alloy 5083 and commercially pure titanium. *Kov Mater* 2016; 54: 71–75.
65. Dhindaw BK, De PS and Jayashree P. Friction stir welding of aluminum alloy 1100 and titanium-Al alloy. In: *ASME 2016 11th international manufacturing science and engineering conference*, 2016, pp. 1–4. Blacksburg, VA: ASME.
66. Ghoghery MS, Asgarani MK, Amini K, et al. Friction stir welding of dissimilar joints between commercially pure titanium alloy and 7075 aluminium alloy. *Trans Famena* 2017; 41: 81–90.
67. Wu AP, Song ZH, Nakata K, et al. Defects and the Properties of the Dissimilar Materials FSW Joints of Titanium Alloy TC4 with Aluminum Alloy 6061. In: *Proceedings of the 1st international joint symposium on joining and welding* (ed H Fujii), Osaka, Japan, 2013, pp. 243–248.
68. Gadakh VS, Shinde VB, Khemnar NS, et al. Application of MOORA method for friction stir welding tool material selection. In: Pawar PM, Ronge BP, Balasubramaniam R, et al. (eds) *Techno-societal 2016, proceedings of the international conference on advanced technologies for societal applications*, 2018, pp. 845–854. Cham: Springer.
69. Kumar N, Yuan W and Mishra RS. Friction stir welding of dissimilar alloys. In: *Friction stir welding of dissimilar alloys and materials*. Oxford: Butterworth-Heinemann, 2015, pp. 43–70.
70. Farias A, Batalha GF, Prados EF, et al. Tool wear evaluations in friction stir processing of commercial titanium Ti-6Al-4V. *Wear* 2013; 302: 1327–1333.
71. Kumar N, Yuan W and Mishra RS. Tool design for friction stir welding of dissimilar alloys and materials. In: *Friction stir welding of dissimilar alloys and materials*. Oxford: Butterworth-Heinemann, 2015, pp. 34–42.
72. Buffa G, Lisi M De, Barcellona A, et al. Material flow analysis in dissimilar friction stir welding of AA2024 and Ti6Al4V butt joints. In: *NUMIFORM 2016, MATEC web of conferences*, 2016, pp. 1–7.
73. Pereira VF, Fonseca EB, Costa AMS, et al. Nanocrystalline structural layer acts as interfacial bond in Ti/Al dissimilar joints produced by friction stir welding in power control mode. *Scr Mater* 2020; 174: 80–86.
74. Buffa G, Lisi M De, Sciortino E, et al. Dissimilar titanium/aluminum friction stir welding lap joints by experiments and numerical simulation. *Adv Manuf* 2016; 4: 287–295.
75. Wei Y, Li J, Xiong J, et al. Joining aluminum to titanium alloy by friction stir lap welding with cutting pin. *Mater Charact* 2012; 71: 1–5.
76. Yu-hua C, Quan NI and Li-ming KE. Interface characteristic of friction stir welding lap joints of Ti/Al dissimilar alloys. *Trans Nonferrous Met Soc China* 2012; 22: 299–304.
77. Delijaicov S, Yakabu DY, De Macedo B, et al. Characterization of the surface and mechanical properties of the friction stir welding in tri-dissimilar joints with aluminum alloys and titanium alloy. *Int J Adv Manuf Technol* 2018; 95: 1339–1355.
78. Chen ZW and Yazdanian S. Microstructures in interface region and strengths of friction stir lap Al-to-steel and Al-to-Ti welds. In: Fujii H (ed.) *Proceedings of the 1st international joint symposium on joining and welding*, Osaka, Japan, 2013, pp. 231–235.
79. Zhou L, Yu M, Zhao H, et al. Dissimilar friction stir welding of AA6061 and Ti6Al4V alloys: a study on microstructure and mechanical properties. *J Manuf Process* 2019; 48: 119–126.
80. Yue Y, Zhang Z, Ji S, et al. Friction stir lap welding of 6061-T6 Al to Ti-6Al-4V using low rotating speed. *Int J Adv Manuf Technol* 2018; 96: 2285–2291.
81. Tong L, Xie J, Liu L, et al. Microscopic appraisal and mechanical behavior of hybrid Cu/Al joints fabricated via friction stir spot welding-brazing and modified

friction stir clinching-brazing. *J Mater Res Technol* 2020; 9: 13239–13249.
82. Plaine AH, Suhuddin UFH, Afonso CRM, et al. Interface formation and properties of friction spot welded joints of AA5754 and Ti6Al4V alloys. *Mater Des* 2016; 93: 224–231.
83. Vacchi GS, Plaine AH, Silva R, et al. Effect of friction spot welding (FSpW) on the surface corrosion behavior of overlapping AA6181-T4/Ti-6Al-4V joints. *Mater Des* 2017; 131: 127–134.
84. Asmael MBA and Glaissa MAA. Effects of rotation speed and dwell time on the mechanical properties and microstructure of dissimilar aluminum-titanium alloys by friction stir spot welding (FSSW). *Materwiss Werksttech* 2020; 51: 1002–1008.
85. Huang G and Shen Y. The effects of processing environments on the microstructure and mechanical properties of the Ti/5083Al composites produced by friction stir processing. *J Manuf Process* 2017; 30: 361–373.
86. Mathur V, B SRP, Patel G. C M, et al. Reinforcement of titanium dioxide nanoparticles in aluminium alloy AA 5052 through friction stir process. *Adv Mater Process Technol* 2019; 5: 329–337.
87. Khodabakhshi F, Marzbanrad B, Jahed H, et al. Interfacial bonding mechanisms between aluminum and titanium during cold gas spraying followed by friction-stir modification. *Appl Surf Sci* 2018; 462: 739–752.
88. Bang HS, Bang HS, Song HJ, et al. Joint properties of dissimilar Al6061-T6 aluminum alloy/Ti-6%Al-4%V titanium alloy by gas tungsten arc welding assisted hybrid friction stir welding. *Mater Des* 2013; 51: 544–551.
89. Evans WT, Cook GE and Strauss AM. Joining aerospace aluminum 2024-T4 to titanium by *friction stir extrusion*. In: Yuri H, Mishra R, Sato Y, et al. (eds) *Friction stir welding and processing IX. Pittsburgh, PA:* The Minerals, Metals & Materials Society, 2017, pp. 79–89.
90. Vacchi GS, Silva R, Plaine AH, et al. Refill friction stir spot welded AA5754-H22/Ti-6Al-4V joints: Microstructural characterization and electrochemical corrosion behavior of aluminum surfaces. *Mater Today Commun* 2020; 22: 100759.
91. Kumar S, Wu CS, Padhy GK, et al. Application of ultrasonic vibrations in welding and metal processing: a status review. *J Manuf Process* 2017; 26: 295–322.
92. Evans WT, Gibson BT, Reynolds JT, et al. Friction stir extrusion: a new process for joining dissimilar materials. *Manuf Lett* 2015; 5: 25–28.
93. Wei Y, Aiping W, Guisheng Z, et al. Formation process of the bonding joint in Ti/Al diffusion bonding. *Mater Sci Eng A* 2008; 480: 456–463.
94. Alhazaa AN and Khan TI. Diffusion bonding of Al7075 to Ti-6Al-4V using Cu coatings and Sn-3.6Ag-1Cu interlayers. *J Alloys Compd* 2010; 494: 351–358.
95. Grigor'Evskii VI, Akinin VK and Grigor'Evskaya RV. Diffusion bonding AMg6 aluminium alloy to OT4 titanium alloy through a titanium-aluminium composite interlayer. *Weld Int* 1993; 7: 56–58.
96. AlHazaa A, Khan TI and Haq I. Transient liquid phase (TLP) bonding of Al7075 to Ti-6Al-4V alloy. *Mater Charact* 2010; 61: 312–317.
97. Winiowski A and Majewski D. Brazing of titanium with aluminium alloys. *Arch Metall Mater* 2017; 62: 763–770.
98. Chang SY, Tsao LC, Lei YH, et al. Brazing of 6061 aluminum alloy/Ti-6Al-4V using Al-Si-Cu-Ge filler metals. *J Mater Process Technol* 2012; 212: 8–14.
99. Winiowski A and Różański M. Diffusive brazing of titanium and its alloys with aluminium in the TiAl (γ) phase matrix. *Weld Int* 2011; 25: 331–335.
100. Zhang CQ, Robson JD and Prangnell PB. Dissimilar ultrasonic spot welding of aerospace aluminum alloy AA2139 to titanium alloy TiAl6V4. *J Mater Process Technol* 2016; 231: 382–388.
101. Balle F and Magin J. Solid state joining of aluminium to titanium by high power ultrasonics. *Mater Sci Forum* 2014; 794–796: 345–350.
102. Magin J and Balle F. Solid state joining of aluminum, titanium and their hybrids by ultrasonic torsion welding. *Materwiss Werksttech* 2014; 45: 1072–1083.
103. Marya M, Marya S and Priem D. On the characteristics of electromagnetic welds between aluminium and other metals and alloys. *Weld World* 2005; 49: 74–84.
104. Psyk V, Gershteyn G, Demir OK, et al. Process analysis and physical simulation of electromagnetic joining of thin-walled parts. In: *Proceedings of the 3rd international conference on high speed forming ICHSF—2008*, Dortmund, 2008, pp. 181–190.
105. Way M, Willingham J and Goodall R. Brazing filler metals. *Int Mater Rev* 2020; 65: 257–285.
106. Suslov AA. Brazing laminated structures of light alloys based on aluminium and titanium. *Weld Int* 1995; 9: 570–572.
107. Nesterov AF, et al. Formation of brazed joints in titanium brazed with an aluminium brazing alloy. *Weld Int* 1990; 4: 213–215.
108. Sapanathan T, Raoelison RN, Buiron N, et al. Magnetic pulse welding: an innovative joining technology for similar and dissimilar metal pairs. In: *Joining technologies*, 2016. Epub ahead of print 2016. DOI: 10.5772/63525.
109. Kahraman N, Gulenc B and Findik F. Corrosion and mechanical-microstructural aspects of dissimilar joints of Ti-6Al-4V and Al plates. *Int J Impact Eng* 2007; 34: 1423–1432.
110. Gurevich LM, Trykov YP and Kiselev OS. Formation of structural and mechanical inhomogeneities in explosion welding of aluminium to titanium. *Weld Int* 2014; 28: 128–132.
111. Trykov YP, Gurevich LM and Gurulev DN. Special features of deformation of explosion-welded, titanium-aluminium composite. *Weld Int* 1999; 13: 567–570.
112. Maier V, Höppel W and Göken M. Nanomechanical behaviour of Al-Ti layered composites produced by accumulative roll bonding. *J Phys: Conf Ser* 2010; 012108.
113. Ng HP, Przybilla T, Schmidt C, et al. Asymmetric accumulative roll bonding of aluminium–titanium composite sheets. *Mater Sci Eng A* 2013; 576: 306–315.
114. Zhou L, Yu M, Liu B, et al. Microstructure and mechanical properties of Al/steel dissimilar welds fabricated by friction surfacing assisted friction stir lap welding. *J Mater Res Technol* 2020; 9: 212–221.

115. Ji SD, Wen Q and Li ZW. A novel friction stir diffusion bonding process using convex-vortex pin tools. *J Mater Sci Technol* 2020; 48: 23–30.
116. Wang T, Sidhar H, Mishra RS, et al. Friction stir scribe welding technique for dissimilar joining of aluminium and galvanised steel. *Sci Technol Weld Join* 2018; 23: 249–255.
117. Huang Y, Wan L, Meng X, et al. Probe shape design for eliminating the defects of friction stir lap welded dissimilar materials. *J Manuf Process* 2018; 35: 420–427.
118. Huang Y, Wan L, Si X, et al. Achieving high-quality Al/steel joint with ultrastrong interface. *Metall Mater Trans A Phys Metall Mater Sci* 2019; 50: 295–299.
119. Fuse K and Badheka V. Bobbin tool friction stir welding: a review. *Sci Technol Weld Join* 2019; 24: 277–304.
120. Meng X, Huang Y, Cao J, et al. Recent progress on control strategies for inherent issues in friction stir welding. *Prog Mater Sci* 2021; 115: 100706.
121. Huang Y, Huang T, Wan L, et al. Material flow and mechanical properties of aluminum-to-steel self-riveting friction stir lap joints. *J Mater Process Technol* 2019; 263: 129–137.
122. Huang Y, Wang J, Wan L, et al. Self-riveting friction stir lap welding of aluminum alloy to steel. *Mater Lett* 2016; 185: 181–184.
123. Tutum CC and Hattel J. State-of-the-art multi-objective optimisation of manufacturing processes based on thermo-mechanical simulations. In: Wang L, Ng AHC and Deb K (eds) *Multi-objective evolutionary optimisation for product design and manufacturing*. London: Springer London, 2011, pp. 71–133.